Dynamical Dark Energy Meets Varying Electron Mass: Implications for Phantom Crossing and the Hubble Constant

Adam Smith,^{1,*} Emre Özülker,^{1,†} Eleonora Di Valentino,^{1,‡} and Carsten van de Bruck^{1,§}

¹School of Mathematical and Physical Sciences, University of Sheffield,

Hounsfield Road, Sheffield S3 7RH, United Kingdom

(Dated: October 28, 2025)

We investigate the interplay between varying electron mass (m_e) and dynamical dark energy by analysing the Chevallier-Polarski-Linder (CPL) parametrization and its non-crossing variants, both with and without a varying- m_e component. Our aim is to assess whether the preference for late-time dynamics and phantom divide line (PDL) crossing persists when early-time physics is introduced, and whether these combined models improve the alleviation of the Hubble tension compared to the varying- m_e extension alone. Using the latest CMB, BAO, and supernova datasets, we derive updated constraints on Λ CDM, CPL, and their extensions, and examine their impact on H_0 and the preference for late-time dynamics. We find that $\Lambda \text{CDM} + m_e$ yields the largest upward shift in H_0 , while replacing Λ with the CPL parametrization or its non-crossing variants provides modest improvements in the overall fit. The data consistently favour dynamical dark energy and a phantom divide line crossing at scale factors $a_c \simeq 0.6$ –0.9, and these preferences remain robust, though somewhat weaker ($\gtrsim 2\sigma$), when the electron mass is also allowed to vary. Among the late-time models, CPL performs better than its non-crossing variants, further reinforcing the evidence for a genuine phantom divide crossing. The alleviation of the H_0 tension in the varying- m_e case arises from late-time data breaking the strong Ω_m - m_e degeneracy in the CMB, while the additional degrees of freedom in CPL models allow the late-time dynamics to absorb this impact, thereby weakening the degeneracy breaking and further lowering H_0 through their ability to yield a decreasing dark energy contribution.

I. INTRODUCTION

The persistent discrepancy between the value of the Hubble constant H_0 inferred from the cosmic microwave background (CMB) within ΛCDM and that measured by late-time distance-ladder methods remains one of the most significant challenges in modern cosmology [1– While ΛCDM anchored on Planck 2018 data yields $H_0 = 67 \pm 0.5 \,\mathrm{km} \,\mathrm{s}^{-1} \,\mathrm{Mpc}^{-1}$ [16], the combination of the independent CMB datasets from SPT+ACT provides $H_0 = 66.59 \pm 0.46 \,\mathrm{km \, s^{-1} \, Mpc^{-1}}$ [17]. On the distance-ladder side, the original SH0ES calibration of supernova distances with Cepheids yielded $H_0 =$ $73.04 \pm 1.04 \,\mathrm{km} \,\mathrm{s}^{-1} \,\mathrm{Mpc}^{-1}$ [18], establishing a > 5σ The latest SH0ES determination, including an additional geometric anchor, reports $H_0 = 73.17 \pm$ $0.86 \,\mathrm{km} \,\mathrm{s}^{-1} \,\mathrm{Mpc}^{-1}$ [19], raising the discrepancy to more than 6.7σ when compared with the new SPT+ACT CMB measurement. This persistent mismatch is robust across different teams, calibrators, and Hubble-flow objects on the distance-ladder side [19-47], as well as among independent analyses probing different scales of the CMB temperature and polarization power spectra [16, 17, 48– 50. It has motivated a wide range of theoretical extensions of the standard cosmological model, targeting both early- and late-time physics, referring respectively

to modifications of the expansion history before and after recombination (see, for example, [5, 10, 51–164]).

Although modifications to early-time physics currently appear to be the most promising avenue for addressing the H_0 tension, an additional and independent discrepancy within the Λ CDM framework has emerged. This tension, unrelated to the H_0 problem, became apparent with the first data release of the Dark Energy Spectroscopic Instrument (DESI) [165, 166] and reignited interest in the possibility of late-time dynamical dark energy [146, 154–158, 165–220]. When DESI baryon acoustic oscillation (BAO) data were combined with CMB measurements, the results favored a deviation from a cosmological constant at the 2.6σ level, which increased to 2.5– 3.9σ when supernova apparent magnitudes were also included [165]. In the second data release, DESI DR2, substantial effort was devoted to identifying potential systematics behind this discrepancy; however, the tension only intensified, reaching 3.1σ for the BAO+CMB combination and rising to $2.8-4.2\sigma$, depending on the supernova compilation used [166].

On the early-time side, modifications of recombination and pre-recombination physics that shrink the sound horizon at last scattering can raise the inferred H_0 [161, 221]. Among these, varying electron mass (m_e) models have emerged as particularly effective [119, 120, 160, 162–164, 222–226], since they coherently rescale all relevant CMB distance scales $(r_s, r_D, r_{\rm eq})$, preserving their ratios and thereby maintaining an excellent fit to the acoustic peak pattern while allowing for a smaller sound horizon that scales the distance measurements from BAO and the distance to the last-scattering surface simultaneously,

 $^{^* \} asmith 69@sheffield.ac.uk$

 $^{^{\}dagger}$ e.ozulker@sheffield.ac.uk

[‡] e.divalentino@sheffield.ac.uk

[§] c.vandebruck@sheffield.ac.uk

yielding a higher H_0 value in better agreement with the local distance measurements.

On the late-time side, dynamical dark energy has been extensively studied as an alternative to a cosmological constant. The Chevallier-Polarski-Linder (CPL) parametrisation [227, 228] provides a minimal twoparameter extension to Λ CDM by replacing the cosmological constant with a barotropic perfect fluid whose dynamical equation-of-state (EoS) parameter is allowed to deviate from w = -1, which is associated with Λ . It is a rich parametrisation that can capture a wide variety of dynamical dark energy phenomenology despite its simplicity. The EoS parameter of CPL, being a linear function of the scale factor in the metric, naturally accommodates EoS evolutions that cross the phantom divide line (PDL), w = -1. Interestingly, the region of the parameter space where the PDL crossing occurs is the one preferred by data combinations including the DESI BAO measurements. While this feature is commonly encountered in the literature when dark energy is treated as an effective term encompassing all possible deviations from ΛCDM (see, e.g., Ref. [175]), it cannot be realized by a minimally coupled scalar field [229]. This limitation has motivated discussions on whether a dynamical dark energy model evolving similarly to CPL but without crossing the PDL, such as the thawing or freezing field scenarios [230, 231], could perform comparably well or even better, and whether the apparent preference for PDL crossing is merely an artifact of the CPL form itself [157, 168, 182, 232–239]. In particular, Ref. [157] introduced two modified versions of the CPL parametrisation that remove the PDL-crossing behaviour, namely $\mathrm{CPL}_{< a_c}$ (capturing freezing fields) and $\mathrm{CPL}_{> a_c}$ (capturing thawing fields), and found that the PDL-crossing feature is genuinely favored by current data, a result that we further investigate in this work by including these models in our analyses.

Most existing analyses of the available cosmological data have examined early- and late-time mechanisms in isolation; yet the absence of a convincing resolution to the cosmological tensions has led to approaches where deviations from the standard model at early and late times are combined [164, 174, 240-248]. The two can interact non-trivially: the same degeneracies that make them promising separately can either lead to improved consistency across datasets or, conversely, cancel out when combined. In fact, Ref. [164] studied the varying- m_e model in combination with $\Lambda_s CDM$ [132–135] (an effectively late-time modification with a sign-switching cosmological constant) and found that the models do not cooperate, and their combination can perform worse than the individual models. This motivates a systematic study of whether the promising early-time extension of a varying m_e can be made more effective when combined with a smoothly evolving dark energy.

In the present work, our main objective is to analyze the non-crossing CPL variants of Ref. [157] alongside the original model, with and without the presence of a varying m_e , to investigate whether the preference for PDL crossing persists and to determine whether any of these combined models offer improved amelioration of the H_0 tension—particularly beyond what the varying- m_e extension can achieve on its own. Thus, we present the latest comprehensive constraints on Λ CDM and Λ CDM + varying- m_e using Planck 2018 [16], Λ CT DR6 lensing [249] and SPT-3G data [250], DESI DR2 [251] or SDSS BAO [252], and Pantheon+ supernovae [253]. We then extend the analysis to CPL and non-crossing CPL variants [227, 228, 230], both with and without varying- m_e .

The remainder of this paper is organised as follows. In Section II, we review the two classes of extensions we investigate: varying- m_e as an early-time mechanism, and CPL (together with its non-crossing variants) as latetime parametrisations of dynamical dark energy. We outline their theoretical motivation and observational challenges. In Section III, we describe the implementation of these models in CLASS, the MCMC methodology, and the dataset combinations employed, including *Planck*, ACT, SPT, DESI DR2/SDSS BAO, and Pantheon+. Our main results are presented in Section IV, where we constrain $\Lambda CDM + varying-m_e$, $CPL + varying-m_e$, and noncrossing CPL + varying- m_e against the chosen datasets, quantify the impact on H_0 and Ω_m , and highlight improvements in fit quality relative to Λ CDM. We also assess the robustness of the preferred $m_e/m_{e,0}$ shift and the resilience of the phantom-divide crossing. Finally, Section V summarises our findings.

II. MODELS

We consider two classes of extensions to the Λ CDM framework. The first is an early-time modification, in which the electron mass is allowed to differ at early times [119, 120, 160], thereby altering the physics of recombination. The second class consists of late-time dark energy extensions, namely the CPL parametrisation [227, 228] and its two non-crossing variants [157], which enable us to isolate the role of the phantom-divide-line (PDL) crossing behaviour. We analyse these extensions both individually and in combination, allowing us to assess whether late-time dynamics can provide further improvement on the H_0 tension beyond the varying- m_e model alone and whether the observational preference for PDL crossing persists in the presence of early-time modifications.

A. Early-time modification: Varying electron mass

Early-time modifications to the Λ CDM model have been extensively investigated as potential resolutions to the Hubble tension [5, 95–120, 163, 164]. At the heart of these attempts lies a simple empirical fact: the angular size of the sound horizon at last scattering, θ_s , is mea-

sured with exquisite precision by Planck, which enforces a strong anticorrelation between the size of the sound horizon r_s and the present-day Hubble constant H_0 . Geometrically, this angle can be expressed as $\theta_s = r_s/D_M(a_*)$, where r_s is the comoving sound horizon at recombination, $D_M(a_*)$ is the comoving angular diameter distance to last scattering, and a_* is the scale factor at recombination. With θ_s effectively fixed by observations, any change in r_s must be compensated by an equivalent change in $D_M(a_*)$, i.e. $D_M(a_*) \propto r_s$. Crucially, the distance D_M is highly sensitive to H_0 ; for a spatially flat universe,

$$D_M(a) = c \int_a^1 \frac{\mathrm{d}a}{a^2 H(a)},\tag{1}$$

and, in fact, $D_M \propto H_0^{-1}$, with or without spatial curvature, if H_0 is treated as independent of the dimensionless density parameters. Consequently, to raise H_0 , one must reduce the sound horizon r_s , making early-time physics a natural arena in which to search for viable resolutions to the tension.

However, the CMB contains far more information than just θ_s , and not every modification that decreases r_s preserves the remaining acoustic features. Among the various proposals, a scenario with a varying electron mass m_e holds a somewhat special position due to its coherent effect on several key distance scales. Assuming that other well-measured quantities, such as the baryon-to-photon ratio, remain fixed, one finds approximately

$$r_s \propto r_D \propto r_{\rm eq} \propto a_*,$$
 (2)

where r_D is the Silk damping scale and $r_{\rm eq}$ is the horizon size at matter–radiation equality [159–164]. This implies that characteristic ratios such as r_s/r_D are preserved while the sound horizon is shrunk. For a comparison with other widely studied early-time modifications and their impact on these distance scales, see Table I. A crucial component of this coherent rescaling lies in the dependence of the Thomson scattering cross section on the electron mass, $\sigma_T \propto m_e^{-2}$, which would not be shared by an arbitrary modification that simply alters a_* . As a result, the varying- m_e model has proven particularly successful in extending the cosmological parameter space to better accommodate higher H_0 , yielding a genuine upward shift in the posterior values when BAO data are also included on top of the CMB data [5, 120, 159, 160, 162–164, 225].

From a theoretical perspective, variations in m_e can naturally arise in models where a light scalar field couples to the electron Yukawa interaction, producing a time variation in the electron mass as the scalar evolves. This is also a generic feature of conformally coupled scalar—tensor theories, where all dimensionful parameters, including m_e , inherit a direct dependence on the scalar field through the conformal factor [254]. Such variations of fundamental constants have been explored in a wide range of scalar—field theories. In string-inspired dilaton models [255, 256], the scalar couples universally to all gauge fields and Yukawa coupling terms, leading to time variation of both α and m_e . Similar effects arise in generic extra-dimensional scenarios [257–260], where the electron mass inherits time dependence through axionic and dilatonic couplings.

Runaway scalar fields and coupled quintessence scenarios [261–263] can also induce varying fermion masses through couplings to the Higgs sector, with Higgs-portal interactions providing a natural particle-physics realisation [264–266] (see also [267] for a scalar–tensor embedding). Chameleon models [268, 269] and general scalar–tensor theories likewise predict conformal couplings of light scalars, in which all dimensionful parameters, such as the electron mass, rescale with the scalar field. A varying electron mass can therefore be viewed as part of this broader class of varying-constant frameworks, as discussed in [270, 271]. For phenomenological studies, one often parametrises

$$m_e(z) = m_{e,0} (1 + \delta m_e(z)),$$
 (3)

with $m_{e,0} \equiv 511 \, \mathrm{keV}$ being the present-day measured value, and the fractional variation chosen to peak around recombination in order to have maximal impact on the sound horizon.

The electron mass evolution is not without its own possible pitfalls and constraints. Planck data alone actually prefer a shift in the electron mass in the opposite direction to that required to alleviate the Hubble tension. Specifically, they show a mild preference for a *lower* electron mass at early times, which increases the sound horizon r_s rather than decreasing it, as would be desired. The upward shift in H_0 only emerges once BAO data are included: BAO data prefer lower values of Ω_m for a ΛCDM-like late-time expansion, which selects the high- H_0 end of the Ω_m - H_0 degeneracy that follows the tightly constrained CMB relation $\omega_m = \Omega_m h^2 \sim \text{const.}$ In this sense, the CMB alone, despite directly probing the epoch where $m_e \neq m_{e,0}$, does not drive the increase in H_0 . Instead, the varying- m_e extension enlarges the parameter space in a way that allows the BAO-preferred low- Ω_m region to be reached, which is inaccessible in baseline Λ CDM. In addition, variations in m_e affect Big Bang Nucleosynthesis (BBN) [272] and are subject to stringent astrophysical and laboratory bounds on constant variation at low redshift [254], further tightening the viable parameter space. These considerations represent the main obstacle to varying electron-mass models fully resolving the Hubble tension.

There are also significant theoretical challenges. Varying m_e requires a light scalar coupled to the Standard Model, for which the simplest, safest, and best-motivated couplings are approximately universal. If the coupling

 $^{^1}$ Allowing spatial curvature to vary in addition to m_e further enhances this improvement, but we do not include such extensions in this work.

Mechanism	r_s	r_D	$r_{ m eq}$	Main effect
$\overline{\text{varying-}m_e}$	$\propto a_*$	$\propto a_*$	$\propto a_*$	All scales shrink together
EDE	\downarrow	\downarrow (weaker)	\sim	Primarily reduces r_s
$\Delta N_{ m eff}$	\downarrow	\downarrow (weaker)	↑	More damping; higher Y_p
varying- $\alpha/{\rm rates}$	indirect	<u> </u>	~	Damping tail altered

TABLE I. Impact of different early-time modifications on CMB distance scales. A varying electron mass shifts all three scales in lockstep, unlike other models. The symbol \sim indicates quantities that remain approximately unchanged.

is roughly universal, for example arising from a conformal rescaling, dimensionless ratios such as m_p/m_e can remain unchanged, but atomic scales like the Rydberg energy $(E_R \propto m_e \alpha^2)$ and scattering coefficients like the Thomson cross section $(\sigma_T \propto \alpha^2/m_e^2)$ still vary, altering the microphysics of recombination [254]. Even if the proton-electron mass ratio m_p/m_e remains invariant under a universal coupling, nuclear binding energies need not necessarily rescale in the same way. As a result, the relative shifts in m_p , m_e , and the binding energies alter the ratios entering atomic spectra, leading to changes in the frequencies of absorption and emission lines as the scalar evolves, in conflict with stringent astrophysical and laboratory bounds [254]. Departures from strict universality are generic in realistic constructions (e.g., scalar dependence in gauge kinetic terms or nonuniform Yukawa couplings), in which case the QCD scale $\Lambda_{\rm QCD}$ and quark masses may not track m_e , leading to variations in m_p/m_e and in nuclear binding energies that are tightly constrained [270]. Moreover, a light, coupled scalar typically mediates long-range forces and induces composition-dependent accelerations of astrophysical objects, challenging weak-equivalence-principle tests unless screening mechanisms are invoked [268, 269]. Radiative stability is another concern: maintaining a sub-eV scalar mass with appreciable couplings to electrons is technically unnatural without protective symmetries such as scaling or shift symmetries [264–266].

With these observational and theoretical challenges in mind, varying- m_e remains the statistically most promising early-time mechanism to alleviate the Hubble tension, standing out as the only proposal that consistently reduces the discrepancy below 3σ for the datasets considered in this paper [119, 120, 162, 163]. This makes it the best-motivated early-time extension to combine with late-time modifications in the search for a more complete cosmological model. Accordingly, in our implementation, we adopt a simple prescription for the evolution of the electron mass as implemented in CLASS. where the difference term in Eq. (3) reads $\delta m_e(z) =$ $(m_e/m_{e,0}-1)\Theta(z-50)$, with $\Theta(z)$ being the step function, $m_{e,0}$ the present-day value of the electron mass measured to be 511 keV, and m_e a different constant value in the past (z > 50). Hence, the electron mass undergoes a fractional transition relative to its present-day value at a redshift of $z_{\rm sw} = 50$ and beyond, ensuring a spatially

uniform constant shift in the mass across recombination.²

B. Late-time modifications: CPL with and without phantom crossing

Late-time modifications to Λ CDM have been explored extensively in attempts to reconcile the Hubble tension and improve the fit to low-redshift datasets [10, 51– 94, 132]. Despite their variety, most late-time scenarios face the same challenge regarding the local H_0 measurements. BAO measurements, if anchored to the size of the sound horizon given by the Λ CDM-like early universe, strongly restrict the ability of these models to accommodate a higher H_0 . In fact, BAO data calibrated in this way show discordance with the supernova data if their absolute magnitude is chosen to agree with a high H_0 value, independent of the cosmological model; see e.g. Ref. [112]. That said, independent of the H_0 problem, data from established cosmological probes significantly prefer a dynamical dark energy source over a cosmological constant, with a statistical significance of $\gtrsim 3\sigma$.

The observation that late-time modifications are hindered by BAO data when those measurements are calibrated using the Λ CDM sound horizon naturally raises a key, and arguably underexplored, question: can late-time modifications be revived when combined with early-time physics that alter r_s ? In particular, one may ask whether a dynamical dark energy component, when paired with an early-time mechanism that reduces the sound horizon. (i) can retain (or preferably enhance) the improvement in the H_0 tension provided by the early-time modification, and (ii) simultaneously offer a better fit to dataset combinations (which usually include DESI BAO) that favour late-time deviations from a cosmological constant. A related and preceding question to the latter part is whether such deviations from a cosmological constant remain preferred even in the presence of early-time modifications.

As discussed in Section II A, the early-time modification considered in this work is a sudden shift in the electron mass at redshift $z_{\rm sw}=50$. For the late-time

² We also note the recent interesting approach of accounting for spatial variations in the electron density in Ref. [273]. However, this is conceptually distinct from our case, as it arises from expected clumping-induced corrections rather than from variations in fundamental constants.

sector, we study three models: the CPL parametrisation [227, 228] and its two non-crossing variants introduced in Ref. [157]. The CPL model is a linear equation-of-state parametrisation for dark energy that can phenomenologically capture the dynamics of a wide variety of models. It is a natural benchmark for late-time extensions, particularly given that one of our central goals is to assess whether the preference for dynamical dark energy over a cosmological constant (initially observed in analyses of DESI BAO data using CPL [165, 166]) persists when an early-time modification is included.

The two non-crossing variants modify the CPL form without introducing any additional parameters but restrict the evolution to avoid crossing the phantom divide line (PDL). By comparing these restricted models to the standard CPL case, one isolates the impact of PDL crossing specifically. This is an important exercise, as cosmological fits using CPL not only favour dynamical evolution but tend to prefer precisely the region of parameter space exhibiting PDL crossing. This crossing is a generic feature of CPL, but one that cannot be realised by minimally coupled scalar-field models of dark energy. In fact, the two non-crossing variants, namely $\mathrm{CPL}_{< a_c}$ and $CPL_{>a_c}$, can be interpreted as phenomenological representations of freezing and thawing scalar-field scenarios, respectively. Their inclusion is essential to one of the main questions of this work, namely whether the preference for PDL crossing persists once early-time modifications (specifically varying- m_e) are introduced.

It is important to note that none of these late-time models, when considered in isolation, provide a meaningful resolution to the Hubble tension. In fact, in most cases, they exacerbate it. One might therefore question the motivation for combining such late-time models with a promising early-time mechanism like varying- m_e . However, Ref. [164] showed that even combining varying- m_e with Λ_s CDM, a late-time model that does alleviate the tension on its own, led to a combined outcome that performed worse than either individual model and, in terms of the inferred mean value of H_0 , performed even worse than Λ CDM.

The CPL model extends the baseline Λ CDM framework by introducing two additional parameters, w_0 and w_a , replacing the cosmological constant with a barotropic perfect fluid whose equation of state varies linearly with the scale factor,

$$w(a) = w_0 + w_a(1 - a). (4)$$

This functional form generically allows a crossing of the phantom divide, w(a) = -1, at the scale factor

$$a_{\rm c} \equiv 1 + \frac{1 + w_0}{w_a}.\tag{5}$$

The "non-crossing" variants are defined by enforcing w(a) to remain fixed at -1 whenever the vanilla CPL form would otherwise cross the PDL at $a_{\rm c}$, while behaving identically to CPL elsewhere. This leads to two

possibilities, depending on whether the EoS follows CPL before or after the would-be crossing scale,

$$CPL_{>a_{c}}: \quad w(a) = \begin{cases} w_{0} + w_{a}(1-a), & a > a_{c}, \\ -1, & a < a_{c}, \end{cases}$$
 (6)

$$CPL_{\langle a_c}: \quad w(a) = \begin{cases} -1, & a > a_c, \\ w_0 + w_a(1-a), & a < a_c. \end{cases}$$
 (7)

Examples of w(a) evolution for all three models are shown in Fig. 1. In the $CPL_{>a_c}$ model, the EoS is frozen at early times and evolves only after a_c , whereas in $CPL_{\leq a_c}$ it evolves at early times but halts at the phantom divide. These constructions provide controlled departures from Λ while explicitly forbidding phantom crossing and can be regarded as simplified limits of thawing- and freezing-type scalar-field dynamics [230]. In this interpretation, $CPL_{>a_c}$ resembles a thawing scalar field uncoupled from matter: early-time evolution is suppressed by Hubble friction, and dynamics begin only once dark energy dominates [182, 232, 274]. Conversely, $CPL_{< a_c}$ behaves like a freezing scenario in which the field is dynamical at early times and gradually settles toward a constant energy density after a_c [275–277]. Additionally, these parametrisations can phenomenologically describe scalar fields that are coupled to other sectors. For instance, for sufficiently flat potentials, $CPL_{< a_c}$ can mimic the behaviour of a scalar coupled to matter. In such models, the effective potential is shifted by the background density, $V_{\text{eff}}(\phi) = V(\phi) + \rho_m f(\phi)$, so that during matter domination the field is displaced away from its vacuum configuration, producing $w(a) \neq -1$. As the matter density redshifts, the coupling term becomes subdominant and the field relaxes toward the bare potential, causing the equation of state to freeze back to $w \simeq -1$ at late times for sufficiently flat potentials. This qualitative pattern is well known in coupled quintessence and screened scalar scenarios [269, 278–282].

While phenomenologically useful, CPL should not be mistaken for a fundamental scalar-field model. Its perturbations are treated as those of a perfect fluid, whereas in realistic scalar theories the dynamics depend on the kinetic term, potential, and couplings. Vanilla CPL cannot capture richer features such as oscillations, tracking behaviour, or sharp transitions. Its minimality is a strength but also a limitation: it cannot reproduce more complex dynamics such as thawing-freezing transitions, multi-slope potentials, or non-minimal couplings [283–285]. The PDL-crossing behaviour inferred from data may reflect the restrictions of the parametrisation rather than genuine physics, although there is substantial support for the genuineness of the PDL crossing [157, 175, 233, 234, 286–289].

If one assumes a scalar-field origin for the three CPL models, a parallelism arises with the varying electron mass, as it also almost inevitably points to a scalar origin. Since $m_e = y_e v$, with y_e the Yukawa coupling and v the Higgs vacuum expectation value, any cosmological

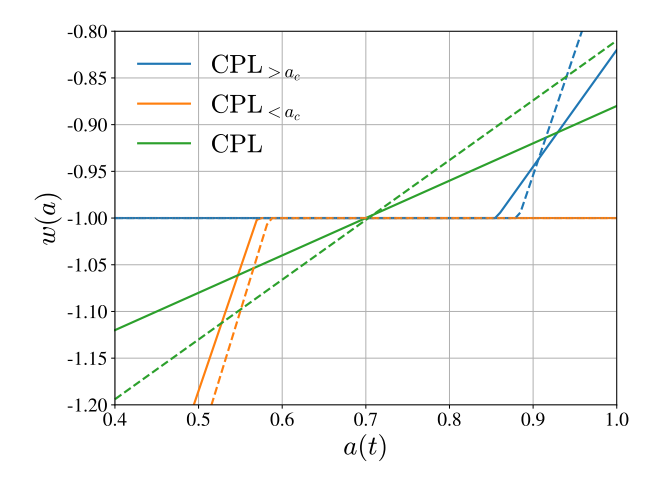


FIG. 1. Evolution of the dark energy equation of state w(a) for the CPL model and its non-crossing variants, shown with and without a varying electron mass. Solid lines correspond to the baseline models, while dashed lines indicate their varying- m_e counterparts. Parameter values are taken from the best fits in Table III, using the CMB-A+DESI+PP dataset.

variation requires promoting one of these parameters to a dynamical field. This mirrors the situation in string- and extra-dimensional frameworks, where effective couplings and particle masses are controlled by moduli whose cosmological evolution induces apparent variations in the "constants." In varying- m_e models, the scalar couples to the electron mass and shifts atomic binding energies, altering the recombination history and the location of the CMB acoustic peaks; however, once recombination is complete, the scalar's effect on late-time dynamics is negligible. In quintessence, by contrast, the scalar contributes directly to the dark-energy sector and can remain dynamical at late times during sustained cosmic acceleration. A natural path could be to consider a single scalar field to drive both modifications in the two different epochs. However, this does not appear to be a straightforward path: attempting to use a single scalar to both source late-time dark energy and induce electronmass variation would generally violate stringent bounds on low-redshift variations of fundamental constants. Two distinct scalar degrees of freedom would therefore seem to be required, which is plausible in many fundamental theories, though at the cost of economy and naturalness.

Despite these caveats, CPL remains the standard benchmark³ for testing late-time dynamics and is a natural candidate to complement early-time mechanisms such as varying- m_e . In what follows, we therefore treat CPL and its non-crossing variants to quantify the interplay between early- and late-time physics in a model-

Model	Parameters	Priors
	$\Omega_b h^2$	[0.005, 0.1]
	$\Omega_c h^2$	[0.001, 0.99]
ΛCDM	$ au_{ m reio}$	[0.01, 0.8]
MODM	A_s	$[5 \times 10^{-10}, 5 \times 10^{-9}]$
	n_s	[0.8, 1.2]
	θ_s	[0.5, 10]
CPL	w_0	[-3, 1]
	w_a	[-3, 2]
$CPL_{>a_c}$		
$CPL_{< a_c}$		
$+m_e$	$m_e/m_{e,0}$	[0.9, 1.1]

TABLE II. Free parameters, their labels, and flat prior ranges, adopted for each model.

independent way.

III. METHODOLOGY & DATASETS

A. Model specifics

In this paper, we consider variations of the CPL model with and without the inclusion of a varying electron mass, as well as constraints on the Λ CDM model combined with a varying- m_e , using the datasets listed in Section III B. The model combinations are summarised in Table II. In addition to the six standard Λ CDM parameters, the varying electron mass models introduce the electron mass rescaling parameter $m_e/m_{e,0}$, and, in CPL-type cases, the dark energy equation-of-state parameters (w_0, w_a) . We impose wide, flat priors on these parameters, as shown in Table II. Appendix Λ discusses the impact of tighter w_a priors, as considered in Ref. [163].

For the electron mass variation, we consider an instantaneous switch publicly available in CLASS: the electron mass is rescaled by a factor $m_e/m_{e,0}$ for all $z>z_{\rm sw}$ and restored to its standard value $m_{e,0}$ for $z < z_{sw}$, thereby satisfying local constraints on the electron mass today. Our baseline choice is to implement this transition at the default redshift $z_{\rm sw} = 50$, i.e. after recombination and deep in the matter-dominated era, so that the primary CMB anisotropies (imprinted at $z \sim 1100$) fully experience the modified m_e , while late-time physics (reionization and below) does not. This choice corresponds to the treatment in [159] and is somewhat arbitrary, since the additional optical depth accumulated in this range is negligible. For the non-crossing CPL cases, we enforce the conditions w(a) = -1 for $a < a_c$ or $a > a_c$ in the CPL_{>a_c} and $CPL_{\langle a_c \rangle}$ models, respectively, by directly modifying

³ Alternative approaches include non-parametric reconstructions of w(z) or model-inspired forms based on specific quintessence or k-essence potentials. These offer greater flexibility but at the cost of additional parameters and reduced interpretability.

⁴ This extension is denoted simply as $+m_e$ throughout the paper.

the equation of state of the fluid-like dark energy component in CLASS from the default CPL implementation. In this way, once the phantom-divide line is reached by the background dark energy equation of state, it remains fixed at w=-1 in the past or future, respectively.

B. Datasets & analysis

We explore our cosmological scenarios across several complementary datasets, spanning early- and late-time probes. In particular, we make use of the following combinations:

Cosmic Microwave Background. We consider two main combinations of CMB datasets:

- Planck+ACT (CMB-A): This dataset includes the full-mission Planck 2018 legacy release [48, 290], using the high-ℓ TT, TE, and EE likelihoods from Plik, together with the low-ℓ TT and EE likelihoods from Commander and SimAll, respectively. We also include the actplanck_baseline v1.2 likelihood, which combines CMB lensing measurements from the Planck PR4 release and the Atacama Cosmology Telescope (ACT) DR6 data [249, 291, 292].
- Planck+ACT+SPT (CMB-B): This combination extends CMB-A by incorporating the new SPT-3G D1 dataset [17], which provides high-resolution measurements of both temperature and polarization anisotropies (TT, TE, EE) and an independent CMB lensing reconstruction (MUSE [293]). The SPT-3G D1 analysis is based on observations of the 1500 deg² SPT-3G Main Field from the 2019–2020 seasons, delivering the deepest ground-based CMB maps to date. The SPT-3G D1 power spectra achieve the tightest constraints on the lensed EE and TE spectra at multipoles $\ell \simeq 1800\text{--}4000$, surpassing ACT DR6 sensitivity at the smallest angular scales. In this work, we employ the sptlite version of the likelihood, which is marginalised over the nuisance parameters and provides a computationally faster implementation without loss of accuracy in the cosmological constraints.

Baryon Acoustic Oscillations. We use baryon acoustic oscillation measurements from either DESI DR2 or the SDSS/eBOSS compilation. We denote these two choices by:

DESI DR2 (DESI): We employ the latest DESI DR2 BAO compilation [294], which provides 16 measurements of D_M/r_d and D_H/r_d over 0.4 < z < 4.2, together with a D_V/r_d point at lower redshifts (0.1 < z < 0.4), as given in Table IV of Ref. [166]. These measurements are derived from a mix of tracers, including ELGs, LRGs, QSOs, and Lyα forest

- data, and represent the most precise BAO distances currently available at low to intermediate redshifts.
- eBOSS/SDSS (SDSS): As an alternative baseline, we adopt the SDSS/eBOSS compilation [295], which includes both isotropic and anisotropic BAO distance and expansion-rate measurements (see Table 3 of Ref. [295]). These data span a range of redshifts and galaxy tracers, providing robust checks on consistency with DESI.

Supernovae. We consider the following compilation of Type Ia supernova data:

• Pantheon+ (PP): We use the Pantheon+ compilation [253], which comprises 1701 light curves corresponding to 1550 unique Type Ia supernovae, spanning the redshift range 0.001 < z < 2.26. This dataset features improved photometric calibration and a comprehensive treatment of systematics relative to earlier releases.

Each dataset combination explored in this work is designed to probe complementary aspects of cosmology. The CMB anisotropies plus lensing likelihoods from *Planck* precisely constrain the acoustic peaks of the CMB, anchoring the main cosmological parameters that govern the matter and radiation content, expansion history, sound horizon, and damping scale. They also provide key sensitivity to the optical depth to reionization and to inflationary parameters, and are included in all dataset combinations (for the list of parameters that vary, see Table II). The addition of high-resolution groundbased data from ACT and SPT extends multipole coverage to $\ell \sim 4000$, sharpening constraints on the damping tail and lensing amplitude—observables that are particularly sensitive to modifications such as a varying electron mass or dynamical dark energy. BAO measurements from DESI or SDSS/eBOSS directly trace the late-time expansion history and are crucial for breaking the geometric degeneracy between H_0 and the sound horizon r_s . Finally, the Pantheon+ sample provides precise distance-redshift measurements from Type Ia supernovae, serving as an independent anchor on the expansion rate at low redshift and completing the combination of earlyand late-time probes used in this work.

Parameter inference is carried out using a modified version of CLASS [296] interfaced with Cobaya [297] for MCMC sampling. We adopt the hmcode prescription for nonlinear corrections, with nonlinear min k max=20, and use HyRec [298] for recombination physics. To handle the generic phantom crossing in the CPL parametrisation, we employ the parametrised post-Friedmann (PPF) framework [299], which prevents the breakdown of the semiclassical fluid description of dark energy and enables a smooth, continuous transition through the phantom-divide line. For the variation of fundamental constants, we use the instantaneous transition prescription described above. Neutrino physics is modelled with $N_{\rm ur}=2.0328$ and $N_{\rm ncdm}=1$, with a total mass of $m_{\nu}=1$

 $0.06\,\mathrm{eV}$. We run multiple independent MCMC chains in parallel and consider them converged once the Gelman–Rubin convergence statistic satisfies R-1<0.03 for all varied cosmological parameters. A conservative burn-in fraction of 30% is discarded to ensure that spurious points in parameter space are not mistakenly retained during the initial sampling phase. Derived parameters such as H_0 , Ω_m , and σ_8 are computed internally from the chains. Posterior distributions, marginal constraints, and triangle plots are analysed using GetDist [300]. Best-fit parameters are identified as the minimum- χ^2 points explored by the converged chains, while best-fit $\Delta\chi^2$ values are obtained by comparison with the corresponding best-fit χ^2 point of the converged Λ CDM chains.

To quantify the level of disagreement with the local distance-ladder measurement, we follow the overlap, or tail-probability, approach to assess tension (see, e.g., [301] for a justification of this method). We compute the statistical tension between our posterior for H_0 and the SH0ES constraint ($H_0 = 73.04 \pm 1.04 \,\mathrm{km\,s^{-1}\,Mpc^{-1}}$ [18], treated as Gaussian), following the standard procedure for evaluating tensions involving non-Gaussian posteriors [302]. Rather than assuming Gaussian posteriors for our chains, we make use of the full posterior distribution: for each MCMC sample $H_0^{(i)}$ with normalized weight w_i , we compute the cumulative distribution function (CDF) of the SH0ES Gaussian at that value. The effective two-tailed probability is then given by

$$p = \sum_{i} w_i \operatorname{CDF}\left(H_0^{(i)}\right), \tag{8}$$

where we assume that the mean H_0 obtained from our chains is lower than the SH0ES mean. This probability is subsequently converted into an equivalent Gaussian significance, which we report as the "tension" in units of σ . This method accounts for any non-Gaussian features in the posterior and provides a robust, model-independent measure of consistency with the SH0ES determination.

IV. RESULTS

In this section, we present the results and constraints obtained from our model implementations in CLASS. We first examine the constraints derived using the CMB-A combination, which represents the more established and widely used dataset for this early-time probe. We combine CMB-A with DESI BAO and supernova data to break the parameter degeneracies introduced by the additional degrees of freedom in our models. To test the robustness of our findings, we also replace the DESI BAO measurements with the SDSS compilation and assess which results remain stable under this change and which exhibit sensitivity to the choice of BAO dataset. The corresponding 68% confidence intervals for the models and dataset combinations of interest are reported in

Table III. We then investigate how these results change when replacing CMB-A with the CMB-B combination, which includes the new SPT-3G D1 data. The addition of SPT provides higher angular resolution but covers a smaller sky area, and it has recently been reported to increase the Hubble tension to the $> 6\sigma$ level [17]. The corresponding results are presented in Table IV.

A. Goodness-of-fit of the models

Including any of the three CPL parametrisations on top of varying- m_e improves the overall fit across all our runs compared to $\Lambda \text{CDM} + m_e$. In contrast, adding the varying- m_e parameter to the CPL models produces only marginal changes in the total χ^2 , with shifts that can occur in either direction depending on the specific dataset combination. The main exception is the $CPL_{>a_c}$ model in the two runs that include SPT data (see Table IV), where the addition of the electron-mass parameter yields a significant improvement of $\Delta \chi^2 > 5$. When comparing the three CPL models among themselves, the vanilla CPL consistently outperforms the two non-crossing variants across all dataset combinations in which DESI BAO measurements are used, both with and without varying m_e . This indicates a robust preference in the data for the PDL-crossing feature.

A number of $CPL+m_e$ variants achieve noticeable improvements in fit relative to the plain ΛCDM baseline, with $\Delta \chi^2_{\rm best}$ decreasing by between about 3 and 9, depending on the model. Specifically, for the CMB-A+DESI+PP combination, we find that $CPL + m_e$ improves by -8.5, $CPL_{>a_c} + m_e$ by -5.3, and $CPL_{<a_c} +$ m_e by -5.1. When using SDSS BAO data (CMB-A+SDSS+PP), the same hierarchy appears but with smaller improvements: $CPL_{\langle a_c \rangle} + m_e$ gives -6.9, CPL + m_e gives -4.3, and $CPL_{>a_c} + m_e$ gives -3.1. For comparison, $\Lambda \text{CDM} + m_e$ achieves only -2.6 and -1.1 for the two dataset combinations, respectively. It is important to note that adding additional parameters naturally allows for some improvement in χ^2 simply due to the increased number of degrees of freedom. The $\Lambda \text{CDM} + m_e$ model introduces one extra parameter, so an improvement of $\Delta \chi^2 \sim 2$ by itself does not indicate a preference for this model when the Akaike Information Criterion (AIC), which penalizes every extra parameter by 2, is considered. Slightly better, the $CPL+m_e$ models include three additional parameters relative to Λ CDM, so improvements larger than $\Delta \chi^2 \simeq 6$ can be considered meaningful. In this context, the observed reduction of χ^2 by up to ~ 8.5 for the CPL+ m_e model indicates an improvement in the goodness of fit sufficient to surpass the Akaike criterion, despite the increased model complexity.

For the cases where the supernova data are excluded (CMB-A+DESI), the additional freedom is rewarded even more strongly, with CPL + m_e improving by -9.5, CPL_{a_c} + m_e by -6.6, and CPL_{a_c} + m_e by -4.4, while Λ CDM+ m_e reaches only -4.2. These gains indicate

TABLE III. Constraints at the 68% confidence level for selected parameters, with best-fit values in parentheses for w_0 and w_a . Results are shown for CMB-A combinations with either DESI or SDSS, with and without PP supernovae. The quantity $\Delta\chi^2_{\rm best}$ is reported relative to the Λ CDM baseline using the same dataset. Compared to CMB-B, the CMB-A combinations favour similar values of $H_0 \simeq 68$ –69 km s⁻¹ Mpc⁻¹ but yield weaker $\Delta\chi^2$ improvements, indicating that CMB-A does not drive a strong preference for CPL extensions. Sensitivity to the BAO choice (DESI vs. SDSS) is most pronounced for CPL_{<ac}, whereas CPL_{>ac} remains more stable, consistent with the trends shown in Fig. 6.

Model	Dataset	$m_e/m_{e,0}$	$H_0({\rm kms^{-1}Mpc^{-1}})$	w_0	w_a	$\Delta\chi^2_{ m best}$
$CPL_{>a_c} + m_e$	CMB-A+DESI+PP CMB-A+SDSS+PP CMB-A+DESI		68.83 ± 0.82 68.40 ± 1.00 $67.9^{+2.7}_{-2.1}$	$\begin{array}{l} -0.811^{+0.11}_{-0.093} \ (-0.69) \\ -0.85^{+0.13}_{-0.10} \ (-0.80) \\ -0.73 \pm 0.28 \ (-0.65) \end{array}$	$w_a < -1.12 (-2.64)$ $w_a < -1.07 (-2.87)$ $w_a < -1.00 (-1.15)$	-5.3 -3.1 -4.4
$CPL_{>a_c}$	CMB-A+DESI+PP CMB-A+SDSS+PP		67.62 ± 0.57 67.29 ± 0.54	$\begin{array}{l} -0.830^{+0.12}_{-0.089} \ (-0.82) \\ -0.89^{+0.12}_{-0.10} \ (-0.72) \end{array}$	$w_a < -1.19 \ (-1.25)$ $w_a < -1.04 \ (-2.62)$	$-0.4 \\ -1.6$
$CPL_{< a_c} + m_e$	CMB-A+DESI+PP CMB-A+SDSS+PP CMB-A+DESI	$\begin{array}{c} 1.0045^{+0.0081}_{-0.0073} \\ 0.9926^{+0.0080}_{-0.0096} \\ 1.0066^{+0.0082}_{-0.0065} \end{array}$	69.15 ± 0.80 67.60 ± 1.10 69.48 ± 0.80	$\begin{array}{l} -0.32^{+0.93}_{-0.33} \ (0.21) \\ -0.18^{+0.36}_{-0.28} \ (-0.24) \\ -0.37^{+1.1}_{-0.29} \ (-0.14) \end{array}$	$\begin{array}{l} w_a < -1.24 \; (\text{-}2.91) \\ w_a < -1.96 \; (\text{-}2.24) \\ w_a < -1.04 \; (\text{-}1.83) \end{array}$	-5.1 -6.9 -6.6
$CPL_{< a_c}$	CMB-A+DESI+PP CMB-A+SDSS+PP		68.74 ± 0.39 68.33 ± 0.58	$\begin{array}{c} -0.15^{+0.49}_{-0.36} (0.13) \\ -0.09^{+0.48}_{-0.37} (0.19) \end{array}$	$w_a < -1.63 \ (-2.63)$ $w_a < -1.71 \ (-2.56)$	$-5.8 \\ -5.9$
$CPL + m_e$	CMB-A+DESI+PP CMB-A+SDSS+PP CMB-A+DESI	$\begin{array}{c} 1.0068 \pm 0.0070 \\ 0.9973^{+0.0091}_{-0.010} \\ 0.9999^{+0.0061}_{-0.0075} \end{array}$	68.25 ± 0.85 67.40 ± 1.10 $63.9^{+1.9}_{-2.6}$	$\begin{array}{c} -0.86 \pm 0.06 \ (-0.81) \\ -0.856^{+0.062}_{-0.070} \ (-0.92) \\ -0.44^{+0.26}_{-0.21} \ (-0.51) \end{array}$	$\begin{array}{c} -0.44^{+0.26}_{-0.24} \ (-0.64) \\ -0.65^{+0.39}_{-0.30} \ (-0.39) \\ -1.69^{+0.68}_{-0.82} \ (-1.45) \end{array}$	-8.5 -4.3 -9.5
CPL	CMB-A+DESI+PP CMB-A+SDSS+PP		67.64 ± 0.60 67.69 ± 0.64	$-0.84 \pm 0.05 (-0.88)$ $-0.86 \pm 0.06 (-0.86)$	$ \begin{array}{c} -0.60^{+0.21}_{-0.19} \ (-0.40) \\ -0.57 \pm 0.25 \ (-0.56) \end{array} $	$-6.9 \\ -5.0$
Λ CDM + m_e	CMB-A+DESI+PP CMB-A+SDSS+PP CMB-A+DESI		69.62 ± 0.69 68.61 ± 0.98 69.85 ± 0.69	- - -	- - -	-2.6 -1.1 -4.2
ΛCDM	CMB-A+DESI+PP CMB-A+SDSS+PP CMB-A+DESI		68.30 ± 0.28 67.63 ± 0.39 68.39 ± 0.29	- - -	- - -	0.0 0.0 0.0

that the extra parameters are statistically tolerated by the data and, in some cases, rewarded with a substantially better fit. The non-crossing CPL variants, in particular, yield more stable improvements across different BAO dataset choices. However, the absolute magnitude of these χ^2 reductions is still not large enough to be regarded as decisive, and, importantly, they do not correspond to an upward shift in H_0 : the lower χ^2 values are accompanied by higher Ω_m and a suppressed H_0 .

B. Impact of the models on the H_0 tension

None of the model variants considered here provide a better resolution of the Hubble tension than the Λ CDM+ m_e model when constrained with the CMB-A+DESI+PP dataset combination. The most promising case remains Λ CDM+ m_e , which yields $H_0 = 69.6 \pm 0.7$, lying at roughly 2.7 σ from the SH0ES determination of $H_0 = 73.04 \pm 1.04$ [18]. Among the CPL variants, the best-performing case in terms of raising H_0 is CPL $_{<a_c}+m_e$, which gives $H_0 = 69.2 \pm 0.8$, corresponding to a 3.0σ tension with SH0ES. As shown in Table III, the various CPL extensions with varying- m_e

perform only marginally worse, yielding slightly lower mean values of H_0 but broader posteriors that partly compensate through increased uncertainties. For instance, for the CMB-A+DESI+PP data, $CPL_{>a_c}+m_e$ gives $H_0 = 68.83 \pm 0.82$, CPL $_{<a_c} + m_e$ gives 69.15 ± 0.80 , and CPL+ m_e gives 68.25 ± 0.85 , showing that the broader error bars somewhat compensate for the smaller means in the CPL model variants. The direction of correlation among the parameters m_e , H_0 , Ω_m , and σ_8 remains the same across all models, indicating that the underlying physical relationships driving these degeneracies are unchanged. For example, while the mean m_e values for $\Lambda \text{CDM} + m_e$ and $\text{CPL}_{>a_c} + m_e$ are nearly identical ($m_e = 1.0107 \pm 0.0050$ vs. 1.0114 ± 0.0051 with CMB-A+DESI+PP), the latter predicts a lower H_0 (68.83 \pm 0.82 vs. 69.62 \pm 0.69), consistent with the higher preferred Ω_m seen in the triangle plot. The mean Ω_m for $\Lambda \text{CDM} + m_e$ is $\Omega_m = 0.2987 \pm 0.0041$, while for $\text{CPL}_{a_c} + m_e$ it is $\Omega_m = 0.3056 \pm 0.0060$. In this respect, we conclude that the CPL models represent a step in the wrong direction regarding late-time modifications that might enhance the ability of a varying- m_e to alleviate the Hubble tension.

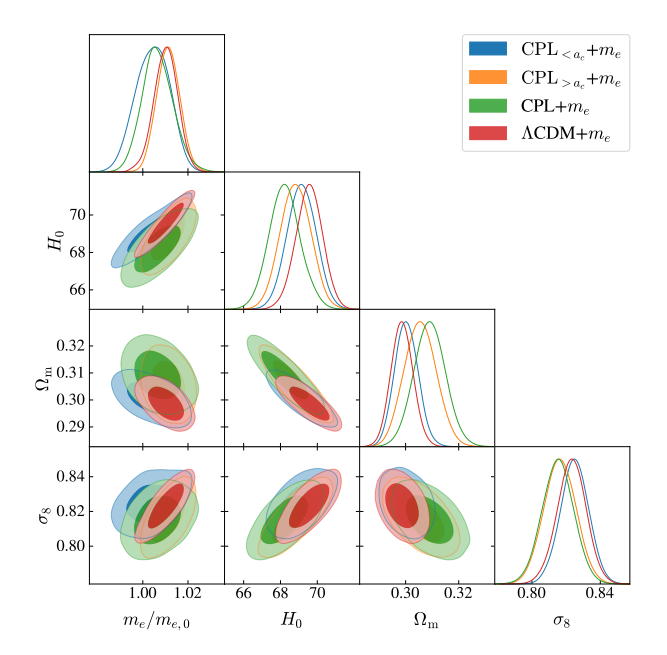


FIG. 2. Triangle plot comparing parameter constraints for the four models with a varying electron mass: $\Lambda \text{CDM} + m_e$, $\text{CPL} + m_e$, $\text{CPL} < a_c + m_e$, and $\text{CPL} > a_c + m_e$. Results are based on the CMB-A+DESI+PP dataset combination, showing that all models share the same correlation directions among m_e , H_0 , Ω_m , and σ_8 but differ in the tightness of their constraints.

C. Why late-time modifications weaken the H_0 alleviation from varying- m_e

We should first understand how the varying- m_e model can address the H_0 tension before investigating the effect of late-time deviations from the cosmological constant when combined. It is natural that the additional uncertainty associated with the extra free parameter $m_e/m_{e,0}$ will enlarge the uncertainty of the constraints on H_0 compared to Λ CDM. This behaviour is generic to any model that extends the standard cosmology but is far from adequate in resolving the tension, particularly when comprehensive datasets are taken into account that break the parameter degeneracies of the models. However, the varying- m_e model also shifts the mean of the H_0 posterior to higher values.

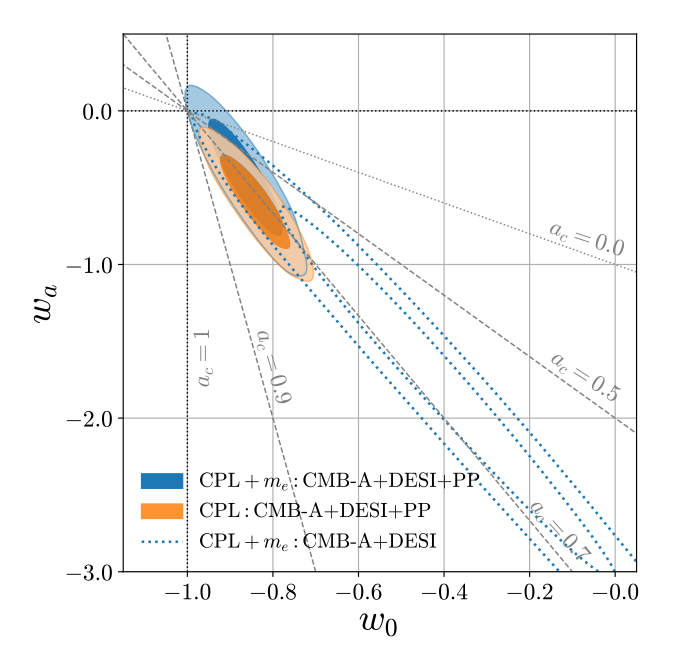
It was discussed in Section II A that a larger electron mass in the early universe can shrink the sound horizon, leading to a higher H_0 value; however, a smaller mass is also allowed in the model, which would worsen the H_0 tension, and it is not immediately clear which region the data would favour. In fact, when the varying- m_e model is constrained using only Planck CMB data, the majority of the posterior volume lies in the $m_e/m_{e,0} < 1$ region, pulling the H_0 constraints down; see, e.g., the results in Refs. [117, 160]. However, when the late-time data, in particular DESI BAO, are included in the dataset on top of the CMB, this situation reverses, and the $m_e/m_{e,0} > 1$ region is preferred or at least contains a significantly

larger portion of the posterior volume, as can be seen in Tables III and IV and also in Fig. 2.

This is closely tied to the anti-correlation between H_0 and the dimensionless matter density parameter $\Omega_m \equiv$ ω_m/h^2 , where ω_m is the physical matter density and h is the reduced Hubble constant, because the impact of late-time data can be interpreted as propagating through this parameter. Ref. [162] finds $m_e/m_{e,0} \propto \omega_m$ in the $\Lambda \text{CDM} + m_e$ model based on precisely constrained CMB observables. Moreover, they find the approximate relation $h \propto \omega_m^{3.23}$, which also yields $\Omega_m \propto (m_e/m_{e,0})^{-5.46}$. This last proportionality makes it clear that a low Ω_m value would lead to a high $m_e/m_{e,0}$, which in turn is able to raise H_0 . Thus, the $\Omega_m - m_e/m_{e,0}$ degeneracy that opens up the parameter space considerably when only the *Planck* CMB data are considered is broken by the DESI BAO data, which by itself prefer low Ω_m values compared to *Planck* within a Λ CDM-like late-time cosmology (compare the results in Tab. 5 of Ref. [166] with Tab. 2 of Ref. [16]). Although Pantheon+ prefers higher Ω_m values by itself [253], the combination of DESI BAO and Pantheon+ as a combined late-time dataset still lies on the lower side compared to the *Planck* CMB results.

Allowing extra degrees of freedom at late times spoils this interplay between the datasets probing different epochs. Although the CPL parametrization yields significantly larger Ω_m values than Λ CDM when constrained by DESI BAO data alone [166], we do not attribute the difference between the H_0 constraints of $\Lambda \text{CDM} + m_e$ and $CPL+m_e$ to this preference for higher Ω_m , since the approximate scaling relation $\Omega_m \propto (m_e/m_{e,0})^{-5.46}$ is model-dependent, and its form is not straightforwardly applicable once late-time dynamics are introduced. Instead, we interpret our results as follows: the extra degrees of freedom in the late-time dynamical models can accommodate the requirements of the DESI BAO data within the dark energy sector itself, rather than these propagating through Ω_m to higher constraints on $m_e/m_{e,0}$. Consequently, the CMB-driven preference for lower $m_e/m_{e,0}$ values is no longer pulled upward as strongly—or, in some cases, not at all—by the complementary constraints of the late-time data. In addition, the quintessence-like behaviour of CPL for $a > a_c$ naturally reduces H_0 due to a decreasing dark energy density right before the present day, and this effect is also present when the electron mass is allowed to vary. It can be seen from Table III that $CPL_{>a_c}$, for which this behaviour is absent, yields slightly higher H_0 values compared to the other two CPL parametrizations, with or without the presence of the varying- m_e .

Finally, we note that since the way varying- m_e alleviates the H_0 tension is through the indirect impact of the late-time data via degeneracy breaking, combining this early modification with simple or minimal late-time dynamics is likely to lead to a weakened alleviation of the H_0 tension. This is also in line with the findings of Ref. [164], where combining varying- m_e with the late-time modification $\Lambda_s \text{CDM}$ [132–135] was counterproduc-



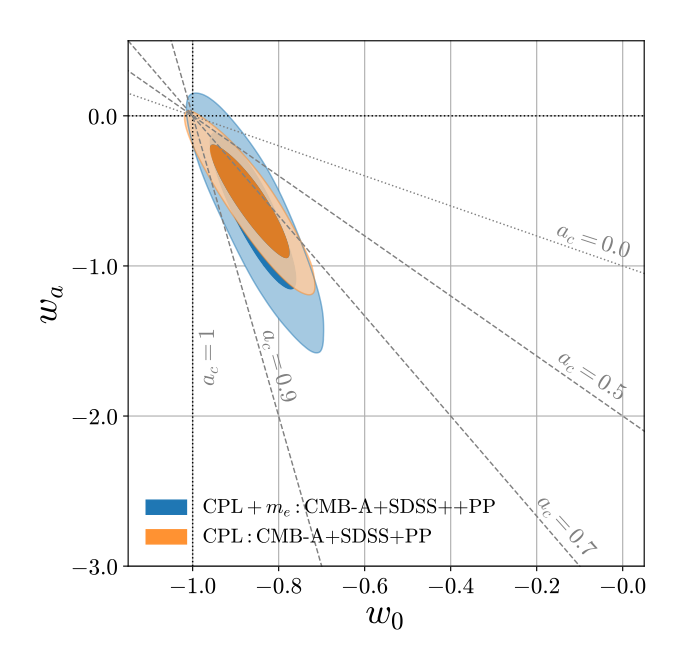


FIG. 3. Comparison of the posterior distributions of the CPL dark energy model with and without a varying electron mass, using CMB-A+PP combined with either DESI BAO (left) or SDSS BAO (right). Two-dimensional contours in the w_0 - w_a plane for CPL+ m_e (blue and dotted blue) and standard CPL (orange), with dashed lines showing example lines of constant crossing scale a_c . Dotted lines illustrate $w_a = 0$ vertically and $w_0 = -1$ horizontally, with the intersection corresponding to w(a) = -1 at all redshifts.

tive in this sense. Still, dynamics that are coupled to the matter sector or non-trivial modifications (e.g., spatial curvature that changes the functional form of the angular diameter distance and is known to work very well in combination with varying- m_e [162]) can prove to be useful. It is also interesting to see whether a similar logic applies to the combination of late-time dynamics with other attempts to address the H_0 tension by modifying the sound horizon rather than the varying- m_e model.

D. Preference for late-time dynamics and PDL crossing in the presence of varying- m_e

In the previous subsection, we examined how introducing late-time CPL dynamics on top of the varying- m_e model impacts the H_0 tension. Here, we take the reverse perspective and investigate how allowing m_e to vary affects the conclusions drawn from the CPL model regarding late-time dynamics.

The effect on the preference for late-time dynamics is summarised in Fig. 3. For the CMB-A+DESI+PP dataset analyses shown in the left panel of the figure, the addition of varying- m_e reduces the preference for dynamical dark energy, as the contours widen due to increased uncertainty and also shift slightly towards the Λ CDM point corresponding to ($w_0 = -1, w_a = 0$); compare the orange CPL contour with the blue CPL+ m_e one. The situation is similar without the inclusion of the Pantheon+ data, as can be seen by comparing the dotted

blue contour of $CPL+m_e$ to the CPL contour in Fig. 11 of Ref. [166]. Still, even when varying- m_e is present, Λ is excluded at $> 2\sigma$, and this exclusion is slightly stronger without the inclusion of the Pantheon+ dataset, as seen from the blue and dotted blue contours in the left panel. In comparison, when DESI BAO is replaced with SDSS BAO, the tension with Λ is not as strong even in the CPL-only case, but curiously, the addition of varying- m_e does not seem to alter the preference for dynamics significantly despite the enlarged uncertainties. The weakening of the preference for late-time dynamics when varying- m_e is present can be attributed to the lack of determination of the sound horizon by the BAO measurements. The distances measured by the BAO teams are unanchored and are proportional to the inverse of the sound horizon at the drag epoch, r_d^{-1} (which changes correspondingly with r_s^{-1} for the discussions considered here), i.e., they measure D_M/r_d , D_H/r_d , and D_V/r_d rather than D_M , D_H , and D_V . Thus, modifying the sound horizon shifts the inferred distances from the BAO data, allowing an additional path to improve the fit of the model on top of modifying the evolution of H(z) with late-time dynamics. This reduces the strength of the need to deviate from Λ at late times to accommodate the BAO data.

An important conclusion is the remarkable resilience of the preference for a phantom-divide crossing. The scale of phantom crossing, a_c , corresponds to a degeneracy line in the w_0 – w_a plane, some examples of which are shown with dashed grey lines in Fig. 3. The degeneracy directions of the CPL contours are altered only

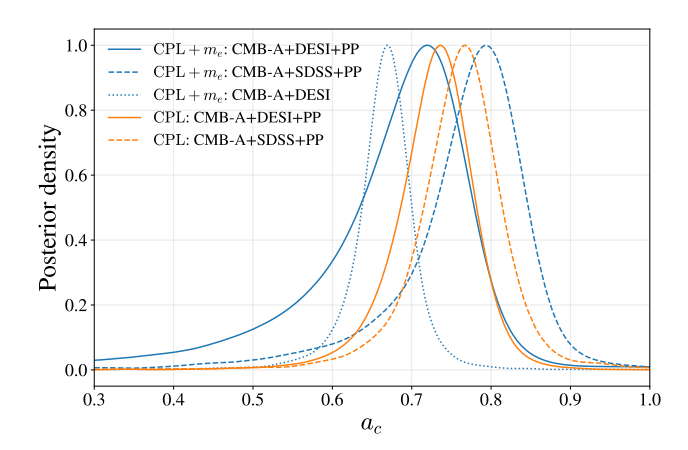


FIG. 4. One-dimensional posterior distributions of the phantom-divide crossing scale factor, $a_{\rm c}$, for the CPL model, shown for different dataset combinations. Solid lines correspond to CMB-A+DESI+PP, dashed lines to CMB-A+SDSS+PP, and dotted lines to CMB-A+DESI. Orange curves represent the base CPL extension, while blue curves show CPL models including a varying electron mass.

minimally by the inclusion of varying- m_e in both the DESI and SDSS analyses. Despite the differing uncertainty sizes and shifts in the contours, they move and deform while closely tracking constant- a_c lines. Since the expansion history of the Universe covers the range 0 < a < 1, a preference for $a_c \in [0,1]$ indicates evidence for phantom crossing. In Fig. 4, we plot the onedimensional marginalised posteriors of the derived parameter a_c with and without varying- m_e , and for both BAO datasets. Regardless of dataset choice or the inclusion of a varying electron mass, all CPL variants exhibit a clear preference for a_c within the relatively narrow range $a_{\rm c} \sim 0.6$ -0.9. Note that this preference does not directly quantify the deviation from Λ , as the cosmological constant corresponding to w(a) = -1 is not distinct from lines of constant a_c . On the contrary, all such lines intersect at the vertex corresponding to the cosmological constant. Hence, this preference for phantom crossing implies that, given the underlying model is not Λ CDM, there is strong evidence for phantom crossing. This point is best illustrated by comparing the dotted blue CPL contour in Fig. 3 with the corresponding dotted blue plot in Fig. 4. Despite the contour being displaced from Λ by slightly more than 2σ , the preference for $a_c \in [0,1]$ seen in Fig. 4 is much stronger; this is because the further the contour lies from Λ , the better it tracks the $a_{\rm c} \sim 0.7$ line.

Another way to quantify the preference for the PDL crossing is by comparing the goodness of fit of the vanilla CPL parametrisation with its non-crossing variants. As shown in Table III, the non-crossing variants perform worse than the vanilla CPL when the DESI BAO data are included in the analyses, with or without the varying- m_e . The fact that dynamical dark energy cannot perform as well when its PDL-crossing feature is removed supports the previous finding that the data favour a PDL cross-

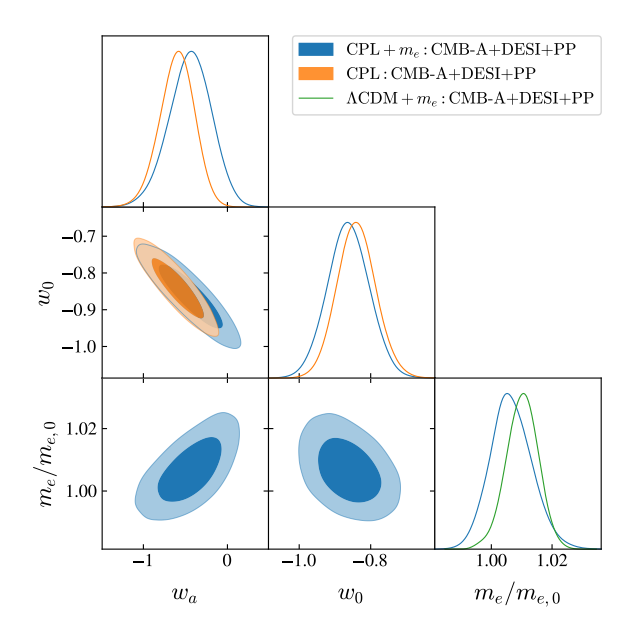


FIG. 5. Triangle plot based on the CMB-A+DESI+PP data combination showing 2D contours and 1D posteriors for $\{w_0, w_a, m_e/m_{e,0}\}$, highlighting correlations in the space of extra free parameters.

ing. When SDSS BAO data are considered, however, the CPL $_{< a_c}$ model performs slightly better. Returning to the DESI BAO case, which is more relevant for discussions of PDL crossing, we see from Table IV that the inclusion of SPT measurements in the CMB data does not change the consistent preference for the vanilla CPL over the non-crossing variants, with or without the varying- m_e . However, the corresponding $\Delta\chi^2$ values are smaller in this case. This weakening of the preference with the inclusion of SPT data is consistent with the findings of Ref. [209], which reported that deviations from Λ CDM towards the region of the w_0 - w_a parameter space with PDL crossing are reduced when one does not restrict the analysis to the Planck CMB data alone.

Finally, we present in Fig. 5 the correlations among all three extra parameters of the $CPL+m_e$ model. In line with the above discussion, we see from the blue contours that when $m_e/m_{e,0}$ agrees with its Λ CDM value $(m_e/m_{e,0}=1)$, the CPL parameters deviate from Λ , and when the CPL parameters agree with their Λ CDM values $(w_0 = -1 \text{ and } w_a = 0)$, the electron mass parameter deviates from unity. From a converse perspective, within the 2σ regions, the further the parameters of either the late- or early-time modifications move away from their ΛCDM values, the closer the other sector is pulled back toward Λ CDM. Altogether, the data indicate that, in the presence of a varying- m_e , late-time deviations from Λ in the form of dynamical dark energy are still preferred, and evidence for PDL crossing persists across analyses. The preferred $a_{\rm c}$ values remain stable across dataset combinations, including the addition of Pantheon+, and even when recombination physics is modified by a varying electron mass. DESI vs SDSS

Different datasets

The role of Pantheon+

An important detail concerns the role of supernova data. As seen in Table III, Pantheon+ provides much of the constraining power for CPL-type models, effectively bringing them back in line with the other CPL variants. Including Pantheon+ in the CMB+BAO combinations both raises the inferred H_0 and narrows the allowed range of late-time equation-of-state parameters. Consequently, the $CPL+m_e$ models can no longer rely on inflated uncertainties to mitigate the Hubble tension. For instance, CPL + m_e constrained by CMB-A+DESI alone yields a low $H_0 = 63.9^{+1.9}_{-2.6} \,\mathrm{km \, s^{-1} \, Mpc^{-1}},$ which increases to $68.25 \pm 0.85 \ \mathrm{km \, s^{-1} \, Mpc^{-1}}$ once Pantheon+ is included. Likewise, $CPL_{>a_c} + m_e$ shifts from $67.9^{+2.7}_{-2.1} \,\mathrm{km}\,\mathrm{s}^{-1}\,\mathrm{Mpc}^{-1}$ to $68.83 \pm 0.82 \,\mathrm{km}\,\mathrm{s}^{-1}\,\mathrm{Mpc}^{-1}$ when Pantheon+ is added. In both cases, the supernova data elevate H_0 towards the SH0ES value, but the simultaneous tightening of the error bars maintains the tension at the $\sim 2.5-3\sigma$ level, comparable to the $\Lambda \text{CDM}+m_e$ case.

It is important to note that the Pantheon+ sample, being uncalibrated, is intrinsically agnostic to the absolute value of H_0 . The absolute distance scale is instead set by the inverse distance ladder through the combination of CMB and BAO data. In this context, Pantheon+ does not itself drive the Hubble tension but reshapes how it appears by tightening degeneracies among late-time parameters. As seen here, adding Pantheon+ to the CMB-A+DESI dataset combination raises the inferred H_0 compared to CMB+DESI alone, while simultaneously narrowing the allowed parameter space. This removes the ability of $CPL+m_e$ models to rely on broad posteriors to ease the tension. In particular, the DESI BAO data tend to favour CPL models that are quintessence-like today $(w_0 > -1)$ and phantom-like in the past $(w_a < 0)$ —a behaviour that drives H_0 to smaller values. The inclusion of Pantheon+ counteracts this trend by pulling the evolution of w(a) closer to -1, thereby restoring an expansion history more consistent with Λ CDM and bringing H_0 back towards its baseline value. By contrast, in standard Λ CDM, the H_0 constraint from CMB+BAO is already very tight ($\sigma_{H_0} \sim 0.3\text{--}0.4 \text{ km s}^{-1} \text{Mpc}^{-1}$), so adding Pantheon+ has little effect on the posterior width. Overall, Pantheon+ strengthens the internal consistency of the fits but removes the flexibility that $CPL+m_e$ models use to weaken the tension, bringing them back to the $\sim 2.5-3\sigma$ discrepancy already present in Λ CDM.

The role of BAO data is particularly revealing when comparing DESI and SDSS inputs. Table III shows that the non-crossing CPL variants respond quite differently to the choice of dataset. For CMB-A+DESI+PP (DESI BAO), $CPL_{\langle a_c + m_e \rangle}$ sits close to $\Lambda CDM + m_e$, with $H_0 \simeq 69.1 \; \mathrm{km} \, \mathrm{s}^{-1} \, \mathrm{Mpc}^{-1}$ and a modest fit improvement $(\Delta \chi^2 \simeq -5)$. However, switching to CMB-A+SDSS+PP (SDSS BAO) drives H_0 down by nearly 1.5 km s⁻¹ Mpc⁻¹ and worsens the relative fit, highlighting its strong sensitivity to the BAO input. By contrast, $CPL_{>a_c} + m_e$ is comparatively stable: the shift in H_0 between DESI and SDSS remains within 0.5 km s⁻¹ Mpc⁻¹, and $\Delta \chi^2$ changes by less than 2, indicating that the "late-evolving" version of the model is much less affected by which BAO compilation is used.

The plain $CPL + m_e$ model also exhibits an interesting trend. With DESI, it yields the lowest H_0 among the variants (68.3 $\rm km\,s^{-1}\,Mpc^{-1}$), while with SDSS the value drops further to 67.4 $\rm km\,s^{-1}\,Mpc^{-1}$, in both cases worsening the tension relative to $\Lambda CDM + m_e$. Meanwhile, the baseline $\Lambda \text{CDM} + m_e$ model itself is remarkably stable across DESI and SDSS, with H_0 shifting by less than $1 \text{ km s}^{-1} \text{ Mpc}^{-1}$ and $\Delta \chi^2$ by less than 2. This contrast highlights that the dataset dependence arises from the impact of the BAO data on the late-time dynamics. The dependence of the CPL parameters on the BAO data is shown in Fig. 3; for the non-crossing variants, we do not plot the contours for the w_0 - w_a parameters due to sharp features in the posteriors (see Fig. 2 of Ref. [157]), but we present the triangular plot of $m_e/m_{e,0}$ with key derived parameters, where the impact of the BAO dataset on H_0 and Ω_m can be clearly seen.

Results with SPT data

The inclusion of SPT data causes the χ^2 gap between the Λ CDM and extended models to further widen, indicating stronger deviations from Λ CDM. However, as discussed in Section IVC, the χ^2 improvements over $\Lambda \text{CDM} + m_e$ obtained by including late-time dynamics are milder compared to the CMB-A case, indicating a reduced preference for late-time dynamics in the presence of this dataset, in line with the findings of Ref. [209].

Without Pantheon+ supernovae, both CPL and $CPL+m_e$ drive H_0 to very low values, around 63–64 km s⁻¹ Mpc⁻¹, with broad posteriors and large fit improvements ($\Delta \chi^2_{\rm best} \simeq -12$). By contrast, CPL_{<ac} + m_e stabilises H_0 near 69.6±0.8 km s⁻¹ Mpc⁻¹ with CMB-B+DESI, yielding $\Delta \chi^2 \simeq -8.8$ and only a 2.6σ tension with SH0ES. This combination of a higher H_0 and a substantially improved fit is particularly noteworthy. For comparison, $\Lambda \text{CDM} + m_e$ also pushes H_0 upward to $70.0 \pm 0.7 \; \mathrm{km} \, \mathrm{s}^{-1} \, \mathrm{Mpc}^{-1}$ but achieves only $\Delta \chi^2 \simeq -7.8$, i.e. a slightly worse fit than $CPL_{\langle a_c} + m_e$.

Including Pantheon+ supernovae sharpens this hier-

TABLE IV. Constraints at the 68% confidence level for selected parameters, with best-fit values in parentheses for w_0 and w_a . Results are shown for CMB-B combinations with and without Pantheon+ supernovae, using DESI BAO data. The quantity $\Delta\chi^2_{\rm best}$ is reported relative to the Λ CDM baseline using the same dataset. Compared to CMB-A, the CMB-B combinations yield slightly higher values of $H_0 \simeq 68$ –69 km s⁻¹ Mpc⁻¹ and consistently stronger $\Delta\chi^2$ improvements, indicating that the inclusion of SPT data enhances the preference for CPL-type extensions. Among these, CPL_{ac} + m_e remains the most stable model across different dataset choices.

Model	Dataset	$m_e/m_{e,0}$	$H_0({\rm kms^{-1}Mpc^{-1}})$	w_0	w_a	$\Delta\chi^2_{ m best}$
$CPL_{>a_c} + m_e$	CMB-B+DESI+PP CMB-B+DESI	$\begin{aligned} 1.0136 \pm 0.0045 \\ 1.0148 \pm 0.0048 \end{aligned}$	$69.03 \pm 0.79 \\ 68.1^{+2.7}_{-2.1}$	$\begin{array}{l} -0.815^{+0.12}_{-0.094} \; (\text{-}0.75) \\ -0.73^{+0.32}_{-0.28} \; (\text{-}0.69) \end{array}$	$w_a < -1.14 \ (-2.04)$ $w_a < -1.06 \ (-1.16)$	$-8.1 \\ -8.0$
$CPL_{>a_c}$	CMB-B+DESI+PP CMB-B+DESI		$67.44_{-0.53}^{+0.63} \\ 68.2_{-1.7}^{+2.3}$	$ \begin{array}{l} -0.844^{+0.13}_{-0.098} \ (-0.72) \\ -0.95^{+0.28}_{-0.24} \ (-1.01) \end{array}$	$w_a < -1.24 \ (-2.78)$ $ \ (-0.05)$	$-0.5 \\ -2.8$
$\overline{\text{CPL}_{< a_c} + m_e}$	CMB-B+DESI+PP CMB-B+DESI	$1.0064^{+0.0080}_{-0.0072} \\ 1.0080^{+0.0082}_{-0.0067}$	69.31 ± 0.78 69.60 ± 0.80	$\begin{array}{c} -0.26^{+0.83}_{-0.35} \ (0.08) \\ -0.29^{+0.95}_{-0.35} \ (0.07) \end{array}$	$w_a < -1.34 \ (-2.60)$ $w_a < -1.20 \ (-2.48)$	$-8.3 \\ -8.8$
$CPL_{\leq a_c}$	CMB-B+DESI+PP CMB-B+DESI		68.75 ± 0.38 68.88 ± 0.40	$\begin{array}{c} -0.11^{+0.38}_{-0.33} \ (0.13) \\ -0.15^{+0.40}_{-0.31} \ (-0.68) \end{array}$	$w_a < -1.80 \ (-2.74)$ $w_a < -1.76 \ (-0.86)$	$-8.2 \\ -9.0$
$\overline{\text{CPL} + m_e}$	CMB-B+DESI+PP CMB-B+DESI	$1.0084^{+0.0061}_{-0.0070} \\ 1.0016^{+0.0056}_{-0.0073}$	$68.37 \pm 0.85 \\ 64.0^{+1.8}_{-2.7}$	$ \begin{array}{c} -0.86 \pm 0.06 \; (-0.88) \\ -0.44^{+0.27}_{-0.21} \; (-0.41) \end{array} $	$-0.46^{+0.26}_{-0.23} (-0.23) -1.70^{+0.66}_{-0.83} (-1.76)$	$-10.2 \\ -11.7$
CPL	CMB-B+DESI+PP CMB-B+DESI		$67.65 \pm 0.59 \\ 63.5^{+1.6}_{-2.1}$	$-0.83 \pm 0.05 \; (-0.89) \\ -0.39^{+0.22}_{-0.19} \; (-0.30)$	$ \begin{array}{l} -0.67^{+0.21}_{-0.19} \ (\text{-}0.37) \\ -1.85 \pm 0.56 \ (\text{-}2.17) \end{array}$	$-9.6 \\ -11.9$
Λ CDM + m_e	CMB-B+DESI+PP CMB-B+DESI	$1.0124 \pm 0.0043 1.0135 \pm 0.0043$		- -	- -	-6.7 -7.8
ΛCDM	CMB-B+DESI+PP CMB-B+DESI		$68.04 \pm 0.26 \ (68.25)$ $68.13 \pm 0.26 \ (68.23)$	- -	<u>-</u>	0.0

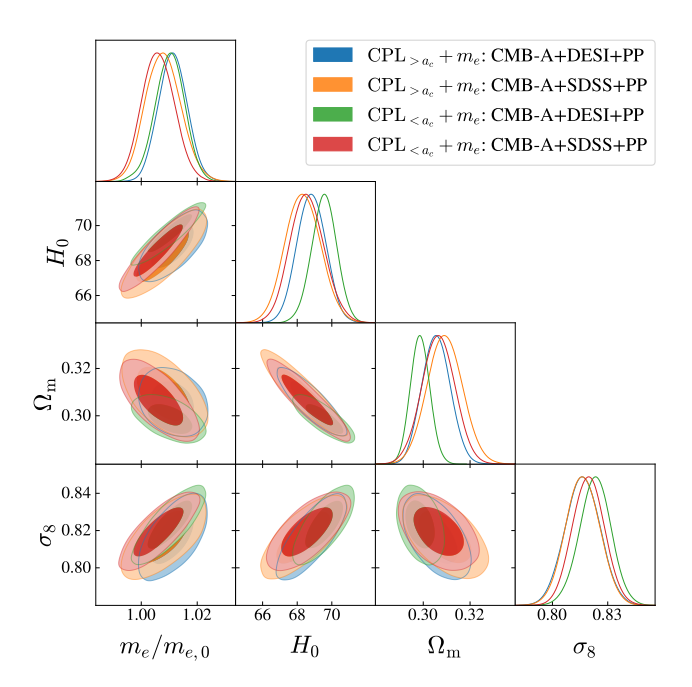


FIG. 6. Triangle plot showing the 2D contour plots and 1D posterior distributions for the $\mathrm{CPL}_{>a_c}+m_e$ and $\mathrm{CPL}_{< a_c}+m_e$ models. Results are shown for CMB-A+PP combined with DESI (green/red) and SDSS (grey/blue) BAO data, highlighting how the early- and late-crossing CPL variants respond differently to the choice of BAO dataset.

archy further. With CMB-B+DESI+PP, CPL $_{<a_c}+m_e$ gives $H_0=69.3\pm0.8~{\rm km\,s^{-1}\,Mpc^{-1}}$ (2.9 σ from SH0ES) and $\Delta\chi^2\simeq-8.3$, while CPL $_{>a_c}+m_e$ yields $H_0=69.0\pm0.8~{\rm km\,s^{-1}\,Mpc^{-1}}$ (3.1 σ) and $\Delta\chi^2\simeq-8.1$. The plain CPL model also achieves strong fit improvements ($\Delta\chi^2\simeq-10$) but at the cost of driving H_0 much lower and pushing w_a to very negative values. Interestingly, the CPL $_{>a_c}$ model benefits most from allowing m_e to vary, with its fit improvement rising from near baseline to competitive with plain CPL, suggesting that modified recombination physics can partially substitute for a late-time phantom crossing.

V. CONCLUSIONS

In this work, we have investigated the interplay between early- and late-time extensions to Λ CDM by combining a varying electron mass with dynamical darkenergy parametrizations. Our primary goals were to examine whether the inclusion of late-time dynamics (incorporated through the CPL model [227, 228] and its non-crossing variants [157]) affects the ability of varying- m_e to alleviate the H_0 tension, and to test whether the preference for deviations from Λ and the phantom-divide line (PDL) crossing observed in dynamical dark energy analyses persists once early-time modifications are introduced. To this end, we presented comprehensive constraints on Λ CDM and its extensions using Planck 2018,

ACT DR6 lensing, and SPT-3G CMB data, in combination with DESI DR2 or SDSS BAO and the Pantheon+supernovae compilation.

Across all dataset combinations analysed, $\Lambda \text{CDM} + m_e$ yields the largest upward shift in H_0 (for example, $H_0 \simeq$ $69.6\pm0.7 \,\mathrm{km}\,\mathrm{s}^{-1}\,\mathrm{Mpc}^{-1}$ for CMB-A+DESI+PP), reducing the tension with SH0ES to about 2.7σ . The CPL parametrisation exacerbates the H_0 tension but provides a better fit to the data compared to varying- m_e , and it consistently favours a late-time crossing of the phantom divide, with $a_c \simeq 0.6-0.9$. This behaviour remains robust when m_e is also allowed to vary: the crossing persists at a similar epoch and with comparable statistical weight, although the overall evidence for dynamical dark energy is weakened. The non-crossing variants, $CPL_{>a_a}$ capturing the phenomenology of thawing scalar field scenarios, and $CPL_{\leq a_c}$ capturing freezing scalar field scenarios, consistently perform worse in their fit to the data compared to the vanilla CPL with phantom crossing when DESI BAO is included in the dataset, whether the electron mass is allowed to vary or not, further supporting evidence for PDL crossing. Results obtained with the CMB-B combination (including SPT-3G D1) follow the same qualitative trends, albeit with weaker preference for dynamical dark energy.

Taken together, our results show that the early-time calibration provided by a percent-level increase in m_e during recombination is chiefly responsible for lifting H_0 . The varying- m_e mechanism alleviates the Hubble tension mainly through the indirect impact of late-time data, which break degeneracies among m_e , Ω_m , and H_0 . When additional degrees of freedom are introduced at late times, as in the CPL extensions, this interplay changes: the dark-energy parameters absorb part of the role previously played by m_e , allowing the distance constraints to be satisfied within the dark-energy sector rather than low Ω_m values that in turn increase $m_e/m_{e,0}$ by degeneracy breaking in a Λ CDM-like cosmology. As a result, the inclusion of late-time dynamics can suppress the upward shift in $m_e/m_{e,0}$, leading to H_0 values that are typically lower than $\Lambda \text{CDM} + m_e$. This interpretation is consistent with Ref. [164], which found that combining varying- m_e with late-time modifications such as Λ_s CDM [132–135] can be counterproductive. Further, in vanilla CPL and $CPL_{>a_c}$, the quintessence-like regime right before the present day has a negative effect on the H_0 tension.

While the CPL parametrisation offers a convenient phenomenological handle on late-time dynamics, its implementation remains inherently ad hoc [303]. The dark-energy sector is treated as a perfect fluid with fixed sound speed, and the stability of phantom-divide crossings is imposed numerically rather than derived from fundamental physics. More consistent approaches—such as scalar-field or effective-field-theory frameworks—determine both the background and perturbation evolution from the underlying dynamics and stability conditions [304], whether motivated by a Lagrangian construction or by more general EFT princi-

ples. Canonical single-field quintessence cannot cross the phantom divide [305, 306], and phantom models introduce ghost instabilities [307, 308], while multi-field or coupled scenarios (e.g. quintom models [309], scalar-tensor extensions [310–312], or beyond-Horndeski theories [313]) can realise smooth CPL-like behaviour across w = -1. Such setups avoid perturbative pathologies but at the cost of substantially modifying both the expansion history and structure formation, reinforcing the need for physically consistent late-time models beyond CPL and motivating their joint exploration with early-time modifications such as varying- m_e , as undertaken in this work.

For the early-time physics, we modelled a step-like variation of the electron mass using the instantaneous varying-constants module of CLASS. Although this provides a practical framework, the step approximation at z=50 is an idealisation that introduces a formal discontinuity in $\sigma_{\rm T} \propto m_e^{-2}$. A smoother evolution of $m_e(z)$ that perhaps changes even during recombination within a fully consistent treatment would offer a more physical implementation and will be explored in future work.

In summary, in a scenario where m_e is also allowed to vary, replacing the cosmological constant with latetime dynamics (in the form of CPL and its variants) can provide modest $\Delta \chi^2$ improvements by exploiting extra flexibility in the expansion history, and they exclude the cosmological constant at $\gtrsim 2\sigma$ with a strong preference for a PDL crossing. The evidence for the PDL crossing is further supported by the underperformance of the non-crossing CPL variants. However, the addition of the late-time dynamics does not further relieve the Hubble tension; rather, it worsens it. Consequently, $\Lambda \text{CDM} + m_e$ remains the configuration that most effectively raises H_0 among those tested. Since varying- m_e alleviates the H_0 tension primarily through degeneracy breaking with latetime data, combining it with minimal dynamical extensions tends to weaken the improvement. More complex modifications, such as couplings to matter (spatial curvature is already known to work well alongside varying m_e [162]), may offer better synergy. It is also intriguing whether similar behaviour would occur when late-time dynamics are paired with other mechanisms that modify the sound horizon, and whether the preference for a dynamical dark energy and phantom crossing persists in those cases.

ACKNOWLEDGMENTS

We thank William Giarè, Daniel Kessler, Nils Schöneberg and Jesus Torrado for their insightful suggestions and extremely useful discussions. EDV is supported by a Royal Society Dorothy Hodgkin Research Fellowship. AS is supported by the W.D. Collins Scholarship. CvdB is supported in part by the Lancaster–Sheffield Consortium for Fundamental Physics under STFC grant: ST/X000621/1. We acknowledge the IT Services at The University of Sheffield for the provision of services for

High Performance Computing. This article is based upon work from the COST Action CA21136 - "Addressing observational tensions in cosmology with systematics and fundamental physics (CosmoVerse)", supported by COST - "European Cooperation in Science and Technology".

- [1] L. Verde, T. Treu, and A. G. Riess, Nature Astron. 3, 891 (2019), arXiv:1907.10625 [astro-ph.CO].
- [2] E. Di Valentino et al., Astropart. Phys. 131, 102605 (2021), arXiv:2008.11284 [astro-ph.CO].
- [3] E. Di Valentino et al., Class. Quant. Grav. 38, 153001 (2021), arXiv:2103.01183 [astro-ph.CO].
- [4] L. Perivolaropoulos and F. Skara, New Astron. Rev. 95, 101659 (2022), arXiv:2105.05208 [astro-ph.CO].
- [5] N. Schöneberg, G. Franco Abellán, A. Pérez Sánchez, S. J. Witte, V. Poulin, and J. Lesgourgues, Phys. Rept. 984, 1 (2022), arXiv:2107.10291 [astro-ph.CO].
- [6] P. Shah, P. Lemos, and O. Lahav, Astron. Astrophys. Rev. 29, 9 (2021), arXiv:2109.01161 [astro-ph.CO].
- [7] E. Abdalla *et al.*, JHEAp **34**, 49 (2022), arXiv:2203.06142 [astro-ph.CO].
- [8] E. Di Valentino, Universe 8, 399 (2022).
- [9] M. Kamionkowski and A. G. Riess, Ann. Rev. Nucl. Part. Sci. 73, 153 (2023), arXiv:2211.04492 [astro-ph.CO].
- [10] W. Giarè, CMB Anomalies and the Hubble Tension (2023), arXiv:2305.16919 [astro-ph.CO].
- [11] J.-P. Hu and F.-Y. Wang, Universe 9, 94 (2023), arXiv:2302.05709 [astro-ph.CO].
- [12] L. Verde, N. Schöneberg, and H. Gil-Marín, A tale of many H₀ (2023), arXiv:2311.13305 [astro-ph.CO].
- [13] E. Di Valentino and D. Brout, eds., *The Hubble Constant Tension*, Springer Series in Astrophysics and Cosmology (Springer, 2024).
- [14] L. Perivolaropoulos, Hubble Tension or Distance Ladder Crisis? (2024), arXiv:2408.11031 [astro-ph.CO].
- [15] E. Di Valentino et al. (CosmoVerse), The CosmoVerse White Paper: Addressing observational tensions in cosmology with systematics and fundamental physics (2025), arXiv:2504.01669 [astro-ph.CO].
- [16] N. Aghanim et al. (Planck), Astron. Astrophys. 641, A6 (2020), arXiv:1807.06209 [astro-ph.CO].
- [17] E. Camphuis *et al.* (SPT-3G), arXiv:2506.20707 [astro-ph.CO] (2025).
- [18] A. G. Riess et al., Astrophys. J. Lett. 934, L7 (2022), arXiv:2112.04510 [astro-ph.CO].
- [19] L. Breuval, A. G. Riess, S. Casertano, W. Yuan, L. M. Macri, M. Romaniello, Y. S. Murakami, D. Scolnic, G. S. Anand, and I. Soszyński, Astrophys. J. 973, 30 (2024), arXiv:2404.08038 [astro-ph.CO].
- [20] W. L. Freedman, B. F. Madore, T. Hoyt, I. S. Jang, R. Beaton, M. G. Lee, A. Monson, J. Neeley, and J. Rich, Astrophys. J. 891, 57 (2020), arXiv:2002.01550 [astro-ph.GA].
- [21] S. Birrer et al., Astron. Astrophys. 643, A165 (2020), arXiv:2007.02941 [astro-ph.CO].
- [22] R. I. Anderson, N. W. Koblischke, and L. Eyer, Astrophys. J. Lett. 963, L43 (2024), arXiv:2303.04790 [astroph.CO].
- [23] D. Scolnic, A. G. Riess, J. Wu, S. Li, G. S. Anand, R. Beaton, S. Casertano, R. I. Anderson, S. Dhawan, and X. Ke, Astrophys. J. Lett. 954, L31 (2023),

- arXiv:2304.06693 [astro-ph.CO].
- [24] D. O. Jones et al., Astrophys. J. 933, 172 (2022), arXiv:2201.07801 [astro-ph.CO].
- [25] G. S. Anand, R. B. Tully, L. Rizzi, A. G. Riess, and W. Yuan, Astrophys. J. 932, 15 (2022), arXiv:2108.00007 [astro-ph.CO].
- [26] W. L. Freedman, Astrophys. J. 919, 16 (2021), arXiv:2106.15656 [astro-ph.CO].
- [27] S. A. Uddin et al., Astrophys. J. 970, 72 (2024), arXiv:2308.01875 [astro-ph.CO].
- [28] C. D. Huang et al., Astrophys. J. 963, 83 (2024), arXiv:2312.08423 [astro-ph.CO].
- [29] S. Li, A. G. Riess, S. Casertano, G. S. Anand, D. M. Scolnic, W. Yuan, L. Breuval, and C. D. Huang, Astrophys. J. 966, 20 (2024), arXiv:2401.04777 [astroph.CO].
- [30] D. W. Pesce et al., Astrophys. J. Lett. 891, L1 (2020), arXiv:2001.09213 [astro-ph.CO].
- [31] E. Kourkchi, R. B. Tully, G. S. Anand, H. M. Courtois, A. Dupuy, J. D. Neill, L. Rizzi, and M. Seibert, Astrophys. J. 896, 3 (2020), arXiv:2004.14499 [astro-ph.GA].
- [32] J. Schombert, S. McGaugh, and F. Lelli, Astron. J. 160, 71 (2020), arXiv:2006.08615 [astro-ph.CO].
- [33] J. P. Blakeslee, J. B. Jensen, C.-P. Ma, P. A. Milne, and J. E. Greene, Astrophys. J. 911, 65 (2021), arXiv:2101.02221 [astro-ph.CO].
- [34] T. de Jaeger, L. Galbany, A. G. Riess, B. E. Stahl, B. J. Shappee, A. V. Filippenko, and W. Zheng, Mon. Not. Roy. Astron. Soc. 514, 4620 (2022), arXiv:2203.08974 [astro-ph.CO].
- [35] Y. S. Murakami, A. G. Riess, B. E. Stahl, W. D. Kenworthy, D.-M. A. Pluck, A. Macoretta, D. Brout, D. O. Jones, D. M. Scolnic, and A. V. Filippenko, JCAP 11, 046, arXiv:2306.00070 [astro-ph.CO].
- [36] W. L. Freedman, B. F. Madore, T. J. Hoyt, I. S. Jang, A. J. Lee, and K. A. Owens, Astrophys. J. 985, 203 (2025), arXiv:2408.06153 [astro-ph.CO].
- [37] A. G. Riess et al., Astrophys. J. 977, 120 (2024), arXiv:2408.11770 [astro-ph.CO].
- [38] C. Vogl et al., No rungs attached: A distance-ladder free determination of the Hubble constant through type II supernova spectral modelling (2024), arXiv:2411.04968 [astro-ph.CO].
- [39] D. Scolnic et al., Astrophys. J. Lett. 979, L9 (2025), arXiv:2409.14546 [astro-ph.CO].
- [40] K. Said et al., Mon. Not. Roy. Astron. Soc. 539, 3627 (2025), arXiv:2408.13842 [astro-ph.CO].
- [41] P. Boubel, M. Colless, K. Said, and L. Staveley-Smith, Mon. Not. Roy. Astron. Soc. 533, 1550 (2024), arXiv:2408.03660 [astro-ph.CO].
- [42] D. Scolnic, P. Boubel, J. Byrne, A. G. Riess, and G. S. Anand, Calibrating the Tully-Fisher Relation to Measure the Hubble Constant (2024), arXiv:2412.08449 [astro-ph.CO].
- [43] S. Li, A. G. Riess, D. Scolnic, S. Casertano, and G. S. Anand, Astrophys. J. 988, 97 (2025), arXiv:2502.05259

- [astro-ph.CO].
- [44] J. B. Jensen, J. P. Blakeslee, M. Cantiello, M. Cowles, G. S. Anand, R. B. Tully, E. Kourkchi, and G. Raimondo, The TRGB-SBF Project. III. Refining the HST Surface Brightness Fluctuation Distance Scale Calibration with JWST (2025), arXiv:2502.15935 [astroph.CO].
- [45] A. G. Riess et al., The Perfect Host: JWST Cepheid Observations in a Background-Free SN Ia Host Confirm No Bias in Hubble-Constant Measurements (2025), arXiv:2509.01667 [astro-ph.CO].
- [46] M. J. B. Newman et al., Tip of the Red Giant Branch Distances to NGC 1316, NGC 1380, NGC 1404, & NGC 4457: A Pilot Study of a Parallel Distance Ladder Using Type Ia Supernovae in Early-Type Host Galaxies (2025), arXiv:2508.20023 [astro-ph.CO].
- [47] R. Stiskalek, H. Desmond, E. Tsaprazi, A. Heavens, G. Lavaux, S. McAlpine, and J. Jasche, 1.8 per cent measurement of H_0 from Cepheids alone (2025), arXiv:2509.09665 [astro-ph.CO].
- [48] N. Aghanim et al. (Planck), Astron. Astrophys. 641, A1 (2020), arXiv:1807.06205 [astro-ph.CO].
- [49] S. Aiola et al. (ACT), JCAP 12, 047, arXiv:2007.07288 [astro-ph.CO].
- [50] T. Louis et al. (ACT), The Atacama Cosmology Telescope: DR6 Power Spectra, Likelihoods and ΛCDM Parameters (2025), arXiv:2503.14452 [astro-ph.CO].
- [51] R. Murgia, S. Gariazzo, and N. Fornengo, JCAP 04, 014, arXiv:1602.01765 [astro-ph.CO].
- [52] A. Pourtsidou and T. Tram, Phys. Rev. D 94, 043518 (2016), arXiv:1604.04222 [astro-ph.CO].
- [53] R. C. Nunes, S. Pan, and E. N. Saridakis, Phys. Rev. D 94, 023508 (2016), arXiv:1605.01712 [astro-ph.CO].
- [54] S. Kumar and R. C. Nunes, Phys. Rev. D 94, 123511 (2016), arXiv:1608.02454 [astro-ph.CO].
- [55] S. Kumar and R. C. Nunes, Phys. Rev. D 96, 103511 (2017), arXiv:1702.02143 [astro-ph.CO].
- [56] E. Di Valentino, A. Melchiorri, and O. Mena, Phys. Rev. D 96, 043503 (2017), arXiv:1704.08342 [astro-ph.CO].
- [57] W. Yang, A. Mukherjee, E. Di Valentino, and S. Pan, Phys. Rev. D 98, 123527 (2018), arXiv:1809.06883 [astro-ph.CO].
- [58] E. Di Valentino, A. Melchiorri, O. Mena, and S. Vagnozzi, Phys. Dark Univ. 30, 100666 (2020), arXiv:1908.04281 [astro-ph.CO].
- [59] W. Yang, E. Di Valentino, O. Mena, S. Pan, and R. C. Nunes, Phys. Rev. D 101, 083509 (2020), arXiv:2001.10852 [astro-ph.CO].
- [60] M. Lucca and D. C. Hooper, Phys. Rev. D 102, 123502 (2020), arXiv:2002.06127 [astro-ph.CO].
- [61] E. Di Valentino and O. Mena, Mon. Not. Roy. Astron. Soc. 500, L22 (2020), arXiv:2009.12620 [astro-ph.CO].
- [62] S. Kumar, Phys. Dark Univ. 33, 100862 (2021), arXiv:2102.12902 [astro-ph.CO].
- [63] R. C. Nunes and E. Di Valentino, Phys. Rev. D 104, 063529 (2021), arXiv:2107.09151 [astro-ph.CO].
- [64] S. Gariazzo, E. Di Valentino, O. Mena, and R. C. Nunes, Phys. Rev. D 106, 023530 (2022), arXiv:2111.03152 [astro-ph.CO].
- [65] A. Bernui, E. Di Valentino, W. Giarè, S. Kumar, and R. C. Nunes, Phys. Rev. D 107, 103531 (2023), arXiv:2301.06097 [astro-ph.CO].
- [66] K. R. Mishra, S. K. J. Pacif, R. Kumar, and K. Bamba, Phys. Dark Univ. 40, 101211 (2023), arXiv:2301.08743

- [gr-qc].
- [67] M. A. van der Westhuizen and A. Abebe, JCAP 01, 048, arXiv:2302.11949 [gr-qc].
- [68] Y. Zhai, W. Giarè, C. van de Bruck, E. Di Valentino, O. Mena, and R. C. Nunes, JCAP 07, 032, arXiv:2303.08201 [astro-ph.CO].
- [69] G. Liu, Z. Zhou, Y. Mu, and L. Xu, Phys. Rev. D 108, 083523 (2023), arXiv:2307.07228 [astro-ph.CO].
- [70] G. A. Hoerning, R. G. Landim, L. O. Ponte, R. P. Rolim, F. B. Abdalla, and E. Abdalla, Constraints on interacting dark energy revisited: implications for the Hubble tension (2023), arXiv:2308.05807 [astro-ph.CO].
- [71] S. Pan and W. Yang, On the interacting dark energy scenarios - the case for Hubble constant tension (2023), arXiv:2310.07260 [astro-ph.CO].
- [72] S. Castello, M. Mancarella, N. Grimm, D. Sobral-Blanco, I. Tutusaus, and C. Bonvin, JCAP 05, 003, arXiv:2311.14425 [astro-ph.CO].
- [73] M. Forconi, W. Giarè, O. Mena, Ruchika, E. Di Valentino, A. Melchiorri, and R. C. Nunes, JCAP 05, 097, arXiv:2312.11074 [astro-ph.CO].
- [74] Y.-H. Yao and X.-H. Meng, Phys. Dark Univ. 39, 101165 (2023).
- [75] G. Garcia-Arroyo, L. A. Ureña López, and J. A. Vázquez, Phys. Rev. D 110, 023529 (2024), arXiv:2402.08815 [astro-ph.CO].
- [76] D. Benisty, S. Pan, D. Staicova, E. Di Valentino, and R. C. Nunes, Astron. Astrophys. 688, A156 (2024), arXiv:2403.00056 [astro-ph.CO].
- [77] E. Silva, U. Zúñiga Bolaño, R. C. Nunes, and E. Di Valentino, Non-Linear Matter Power Spectrum Modeling in Interacting Dark Energy Cosmologies (2024), arXiv:2403.19590 [astro-ph.CO].
- [78] W. Giarè, Y. Zhai, S. Pan, E. Di Valentino, R. C. Nunes, and C. van de Bruck, Phys. Rev. D 110, 063527 (2024), arXiv:2404.02110 [astro-ph.CO].
- [79] H. Bagherian, M. Joseph, M. Schmaltz, and E. N. Sivarajan, Stepping into the Forest: Confronting Interacting Radiation Models for the Hubble Tension with Lyman-α Data (2024), arXiv:2405.17554 [astro-ph.CO].
- [80] M. A. Sabogal, E. Silva, R. C. Nunes, S. Kumar, and E. Di Valentino, Phys. Rev. D 111, 043531 (2025), arXiv:2501.10323 [astro-ph.CO].
- [81] E. Di Valentino, A. Melchiorri, and J. Silk, Phys. Lett. B 761, 242 (2016), arXiv:1606.00634 [astro-ph.CO].
- [82] E. Di Valentino, É. V. Linder, and A. Melchiorri, Phys. Rev. D 97, 043528 (2018), arXiv:1710.02153 [astro-ph.CO].
- [83] K. Dutta, Ruchika, A. Roy, A. A. Sen, and M. M. Sheikh-Jabbari, Gen. Rel. Grav. 52, 15 (2020), arXiv:1808.06623 [astro-ph.CO].
- [84] R. von Marttens, L. Lombriser, M. Kunz, V. Marra, L. Casarini, and J. Alcaniz, Phys. Dark Univ. 28, 100490 (2020), arXiv:1911.02618 [astro-ph.CO].
- [85] E. Di Valentino, A. Mukherjee, and A. A. Sen, Entropy 23, 404 (2021), arXiv:2005.12587 [astro-ph.CO].
- [86] W. Yang, E. Di Valentino, S. Pan, Y. Wu, and J. Lu, Mon. Not. Roy. Astron. Soc. 501, 5845 (2021), arXiv:2101.02168 [astro-ph.CO].
- [87] E. Di Valentino, S. Gariazzo, C. Giunti, O. Mena, S. Pan, and W. Yang, Phys. Rev. D 105, 103511 (2022), arXiv:2110.03990 [astro-ph.CO].
- [88] L. Heisenberg, H. Villarrubia-Rojo, and J. Zosso, Phys. Dark Univ. 39, 101163 (2023), arXiv:2201.11623 [astro-

- ph.CO].
- [89] S. A. Adil, O. Akarsu, E. Di Valentino, R. C. Nunes, E. Özülker, A. A. Sen, and E. Specogna, Phys. Rev. D 109, 023527 (2024), arXiv:2306.08046 [astro-ph.CO].
- [90] A. Lapi, L. Boco, M. M. Cueli, B. S. Haridasu, T. Ronconi, C. Baccigalupi, and L. Danese, Astrophys. J. 959, 83 (2023), arXiv:2310.06028 [astro-ph.CO].
- [91] A. Krolewski, W. J. Percival, and A. Woodfinden, A new method to determine H₀ from cosmological energydensity measurements (2024), arXiv:2403.19227 [astroph.CO].
- [92] D. Bousis and L. Perivolaropoulos, Phys. Rev. D 110, 103546 (2024), arXiv:2405.07039 [astro-ph.CO].
- [93] X. Tang, Y.-Z. Ma, W.-M. Dai, and H.-J. He, Phys. Dark Univ. 46, 101568 (2024), arXiv:2407.08427 [astro-ph.CO].
- [94] M. T. Manoharan, Eur. Phys. J. C 84, 552 (2024).
- [95] V. Poulin, T. L. Smith, T. Karwal, and M. Kamionkowski, Phys. Rev. Lett. 122, 221301 (2019), arXiv:1811.04083 [astro-ph.CO].
- [96] T. L. Smith, V. Poulin, and M. A. Amin, Phys. Rev. D 101, 063523 (2020), arXiv:1908.06995 [astro-ph.CO].
- [97] F. Niedermann and M. S. Sloth, Phys. Rev. D 103, L041303 (2021), arXiv:1910.10739 [astro-ph.CO].
- [98] C. Krishnan, E. Ó. Colgáin, Ruchika, A. A. Sen, M. M. Sheikh-Jabbari, and T. Yang, Phys. Rev. D 102, 103525 (2020), arXiv:2002.06044 [astro-ph.CO].
- [99] G. Ye, J. Zhang, and Y.-S. Piao, Phys. Lett. B 839, 137770 (2023), arXiv:2107.13391 [astro-ph.CO].
- [100] V. Poulin, T. L. Smith, and A. Bartlett, Phys. Rev. D 104, 123550 (2021), arXiv:2109.06229 [astro-ph.CO].
- [101] F. Niedermann and M. S. Sloth, Phys. Rev. D 105, 063509 (2022), arXiv:2112.00770 [hep-ph].
- [102] D. H. F. de Souza and R. Rosenfeld, Phys. Rev. D 108, 083512 (2023), arXiv:2302.04644 [astro-ph.CO].
- [103] V. Poulin, T. L. Smith, G. F. Abellán, J. L. Bernal, M. Escudero, R. Murgia, and M. Raveri, Phys. Rept. 1018, 1 (2023), arXiv:2302.09032 [astro-ph.CO].
- [104] J. S. Cruz, F. Niedermann, and M. S. Sloth, JCAP 11, 033, arXiv:2305.08895 [astro-ph.CO].
- [105] F. Niedermann and M. S. Sloth, New Early Dark Energy as a solution to the H_0 and S_8 tensions (2023), arXiv:2307.03481 [hep-ph].
- [106] S. Vagnozzi, Universe 9, 393 (2023), arXiv:2308.16628 [astro-ph.CO].
- [107] G. Efstathiou, E. Rosenberg, and V. Poulin, Phys. Rev. Lett. 132, 221002 (2024), arXiv:2311.00524 [astro-ph.CO].
- [108] J. L. Červantes-Cota, S. Galindo-Uribarri, and G. F. Smoot, Universe 9, 501 (2023), arXiv:2311.07552 [physics.hist-ph].
- [109] M. Garny, F. Niedermann, H. Rubira, and M. S. Sloth, Phys. Rev. D 110, 023531 (2024), arXiv:2404.07256 [astro-ph.CO].
- [110] W. Giarè, Phys. Rev. D 109, 123545 (2024), arXiv:2404.12779 [astro-ph.CO].
- [111] W. Giarè, J. Betts, C. van de Bruck, and E. Di Valentino, A model-independent test of prerecombination New Physics: Machine Learning based estimate of the Sound Horizon from Gravitational Wave Standard Sirens and the Baryon Acoustic Oscillation Angular Scale (2024), arXiv:2406.07493 [astro-ph.CO].
- [112] V. Poulin, T. L. Smith, R. Calderón, and T. Simon,

- Phys. Rev. D 111, 083552 (2025), arXiv:2407.18292 [astro-ph.CO].
- [113] D. Pedrotti, J.-Q. Jiang, L. A. Escamilla, S. S. da Costa, and S. Vagnozzi, Multidimensionality of the Hubble tension: the roles of Ω_m and ω_c (2024), arXiv:2408.04530 [astro-ph.CO].
- [114] J. Kochappan, L. Yin, B.-H. Lee, and T. Ghosh, Phys. Rev. D 112, 063562 (2025), arXiv:2408.09521 [astro-ph.CO].
- [115] K. L. Greene and F.-Y. Cyr-Racine, JCAP 10, 065, arXiv:2306.06165 [astro-ph.CO].
- [116] K. Greene and F.-Y. Cyr-Racine, Phys. Rev. D 110, 043524 (2024), arXiv:2403.05619 [astro-ph.CO].
- [117] M. Baryakhtar, O. Simon, and Z. J. Weiner, Phys. Rev. D 110, 083505 (2024), arXiv:2405.10358 [astro-ph.CO].
- [118] G. P. Lynch, L. Knox, and J. Chluba, Phys. Rev. D 110, 083538 (2024), arXiv:2406.10202 [astro-ph.CO].
- [119] N. Lee, Y. Ali-Haïmoud, N. Schöneberg, and V. Poulin, Phys. Rev. Lett. 130, 161003 (2023), arXiv:2212.04494 [astro-ph.CO].
- [120] O. Seto and Y. Toda, Phys. Rev. D 110, 083501 (2024), arXiv:2405.11869 [astro-ph.CO].
- [121] E. Di Valentino, R. Z. Ferreira, L. Visinelli, and U. Danielsson, Phys. Dark Univ. 26, 100385 (2019), arXiv:1906.11255 [astro-ph.CO].
- [122] G. Alestas, D. Camarena, E. Di Valentino, L. Kazantzidis, V. Marra, S. Nesseris, and L. Perivolaropoulos, Phys. Rev. D 105, 063538 (2022), arXiv:2110.04336 [astro-ph.CO].
- [123] Ruchika, H. Rathore, S. Roy Choudhury, and V. Rentala, JCAP 06, 056, arXiv:2306.05450 [astro-ph.CO].
- [124] E. Frion, D. Camarena, L. Giani, T. Miranda, D. Bertacca, V. Marra, and O. F. Piattella, Bayesian analysis of a Unified Dark Matter model with transition: can it alleviate the H₀ tension? (2023), arXiv:2307.06320 [astro-ph.CO].
- [125] Ruchika, L. Perivolaropoulos, and A. Melchiorri, Effects of a local physics change on the SH0ES determination of H_0 (2024), arXiv:2408.03875 [astro-ph.CO].
- [126] L. Visinelli, S. Vagnozzi, and U. Danielsson, Symmetry 11, 1035 (2019), arXiv:1907.07953 [astro-ph.CO].
- [127] G. Ye and Y.-S. Piao, Phys. Rev. D 101, 083507 (2020), arXiv:2001.02451 [astro-ph.CO].
- [128] R. Calderón, R. Gannouji, B. L'Huillier, and D. Polarski, Phys. Rev. D 103, 023526 (2021), arXiv:2008.10237 [astro-ph.CO].
- [129] A. A. Sen, S. A. Adil, and S. Sen, Mon. Not. Roy. Astron. Soc. 518, 1098 (2022), arXiv:2112.10641 [astro-ph.CO].
- [130] S. Di Gennaro and Y. C. Ong, Universe 8, 541 (2022), arXiv:2205.09311 [gr-qc].
- [131] Y. C. Ong, Universe 9, 437 (2023), arXiv:2212.04429 [gr-qc].
- [132] O. Akarsu, J. D. Barrow, L. A. Escamilla, and J. A. Vazquez, Phys. Rev. D 101, 063528 (2020), arXiv:1912.08751 [astro-ph.CO].
- [133] O. Akarsu, S. Kumar, N. Özdemir, and M. Sami, Phys. Rev. D 104, 123512 (2021), arXiv:2108.09239 [astro-ph.CO].
- [134] O. Akarsu, S. Kumar, E. Özülker, J. A. Vazquez, and A. Yadav, Phys. Rev. D 108, 023513 (2023), arXiv:2211.05742 [astro-ph.CO].

- [135] O. Akarsu, E. Di Valentino, S. Kumar, R. C. Nunes, J. A. Vazquez, and A. Yadav, Λ_sCDM model: A promising scenario for alleviation of cosmological tensions (2023), arXiv:2307.10899 [astro-ph.CO].
- [136] L. A. Anchordoqui, I. Antoniadis, and D. Lust, Phys. Lett. B 855, 138775 (2024), arXiv:2312.12352 [hep-th].
- [137] O. Akarsu, A. De Felice, E. Di Valentino, S. Kumar, R. C. Nunes, E. Ozulker, J. A. Vazquez, and A. Yadav, Λ_sCDM cosmology from a type-II minimally modified gravity (2024), arXiv:2402.07716 [astro-ph.CO].
- [138] S. Halder, J. de Haro, T. Saha, and S. Pan, Phys. Rev. D 109, 083522 (2024), arXiv:2403.01397 [gr-qc].
- [139] L. A. Anchordoqui, I. Antoniadis, D. Lust, N. T. Noble, and J. F. Soriano, Phys. Dark Univ. 46, 101715 (2024), arXiv:2404.17334 [astro-ph.CO].
- [140] A. Gómez-Valent, A. Favale, M. Migliaccio, and A. A. Sen, Phys. Rev. D 109, 023525 (2024), arXiv:2309.07795 [astro-ph.CO].
- [141] O. Akarsu, A. De Felice, E. Di Valentino, S. Kumar, R. C. Nunes, E. Ozulker, J. A. Vazquez, and A. Yadav, Cosmological constraints on Λ_sCDM scenario in a type II minimally modified gravity (2024), arXiv:2406.07526 [astro-ph.CO].
- [142] A. Yadav, S. Kumar, C. Kibris, and O. Akarsu, Λ_s CDM cosmology: Alleviating major cosmological tensions by predicting standard neutrino properties (2024), arXiv:2406.18496 [astro-ph.CO].
- [143] E. Di Valentino, Mon. Not. Roy. Astron. Soc. 502, 2065 (2021), arXiv:2011.00246 [astro-ph.CO].
- [144] E. Silva, M. A. Sabogal, M. S. Souza, R. C. Nunes, E. Di Valentino, and S. Kumar, New Constraints on Interacting Dark Energy from DESI DR2 BAO Observations (2025), arXiv:2503.23225 [astro-ph.CO].
- [145] E. A. Paraskevas, A. Cam, L. Perivolaropoulos, and O. Akarsu, Phys. Rev. D 109, 103522 (2024), arXiv:2402.05908 [astro-ph.CO].
- [146] M. Scherer, M. A. Sabogal, R. C. Nunes, and A. De Felice, Challenging Λ CDM: 5σ Evidence for a Dynamical Dark Energy Late-Time Transition (2025), arXiv:2504.20664 [astro-ph.CO].
- [147] A. Gomez-Valent and J. Solà Peracaula, Astrophys. J. 975, 64 (2024), arXiv:2404.18845 [astro-ph.CO].
- [148] Ö. Akarsu, L. Perivolaropoulos, A. Tsikoundoura, A. E. Yükselci, and A. Zhuk, Dynamical dark energy with AdS-to-dS and dS-to-dS transitions: Implications for the H_0 tension (2025), arXiv:2502.14667 [astro-ph.CO].
- [149] J. F. Soriano, S. Wohlberg, and L. A. Anchordoqui, Phys. Dark Univ. 48, 101911 (2025), arXiv:2502.19239 [astro-ph.CO].
- [150] M. Bouhmadi-López and B. Ibarra-Uriondo, Cosmographical analysis of sign-switching dark energy (2025), arXiv:2506.12139 [gr-qc].
- [151] S. Pan, W. Yang, E. Di Valentino, A. Shafieloo, and S. Chakraborty, JCAP 06 (06), 062, arXiv:1907.12551 [astro-ph.CO].
- [152] W. Yang, E. Di Valentino, S. Pan, S. Basilakos, and A. Paliathanasis, Phys. Rev. D 102, 063503 (2020), arXiv:2001.04307 [astro-ph.CO].
- [153] W. Yang, E. Di Valentino, S. Pan, A. Shafieloo, and X. Li, Phys. Rev. D 104, 063521 (2021), arXiv:2103.03815 [astro-ph.CO].
- [154] J.-Q. Jiang, D. Pedrotti, S. S. da Costa, and S. Vagnozzi, Non-parametric late-time expansion his-

- tory reconstruction and implications for the Hubble tension in light of DESI (2024), arXiv:2408.02365 [astroph.CO].
- [155] A. Gómez-Valent and J. Solà Peracaula, Phys. Lett. B 864, 139391 (2025), arXiv:2412.15124 [astro-ph.CO].
- [156] E. Specogna, S. A. Adil, E. Ozulker, E. Di Valentino, R. C. Nunes, O. Akarsu, and A. A. Sen, Updated Constraints on Omnipotent Dark Energy: A Comprehensive Analysis with CMB and BAO Data (2025), arXiv:2504.17859 [gr-qc].
- [157] E. Özülker, E. Di Valentino, and W. Giarè, Dark Energy Crosses the Line: Quantifying and Testing the Evidence for Phantom Crossing (2025), arXiv:2506.19053 [astroph.CO].
- [158] D. H. Lee, W. Yang, E. Di Valentino, S. Pan, and C. van de Bruck, The Shape of Dark Energy: Constraining Its Evolution with a General Parametrization (2025), arXiv:2507.11432 [astro-ph.CO].
- [159] L. Hart and J. Chluba, Mon. Not. Roy. Astron. Soc. 474, 1850 (2018), arXiv:1705.03925 [astro-ph.CO].
- [160] L. Hart, J. Chluba, and J. G. Bartlett, Mon. Not. Roy. Astron. Soc. 493, 3255 (2020), arXiv:1912.03986 [astro-ph.CO].
- [161] L. Knox and M. Millea, Phys. Rev. D 101, 043533 (2020), arXiv:1908.03663 [astro-ph.CO].
- [162] T. Sekiguchi and T. Takahashi, Phys. Rev. D 103, 083507 (2021), arXiv:2007.03381 [astro-ph.CO].
- [163] N. Schöneberg and L. Vacher, JCAP 03, 004, arXiv:2407.16845 [astro-ph.CO].
- [164] Y. Toda, W. Giarè, E. Özülker, E. Di Valentino, and S. Vagnozzi, Phys. Dark Univ. 46, 101676 (2024), arXiv:2407.01173 [astro-ph.CO].
- [165] A. G. Adame et al. (DESI), JCAP 02, 021, arXiv:2404.03002 [astro-ph.CO].
- [166] M. Abdul Karim et al. (DESI), DESI DR2 Results II: Measurements of Baryon Acoustic Oscillations and Cosmological Constraints (2025), arXiv:2503.14738 [astroph.CO].
- [167] M. Cortês and A. R. Liddle, JCAP 12, 007, arXiv:2404.08056 [astro-ph.CO].
- [168] D. Shlivko and P. J. Steinhardt, Phys. Lett. B 855, 138826 (2024), arXiv:2405.03933 [astro-ph.CO].
- [169] O. Luongo and M. Muccino, Astron. Astrophys. 690, A40 (2024), arXiv:2404.07070 [astro-ph.CO].
- [170] W. Yin, JHEP **05**, 327, arXiv:2404.06444 [hep-ph].
- [171] I. D. Gialamas, G. Hütsi, K. Kannike, A. Racioppi, M. Raidal, M. Vasar, and H. Veermäe, Interpreting DESI 2024 BAO: late-time dynamical dark energy or a local effect? (2024), arXiv:2406.07533 [astro-ph.CO].
- [172] B. R. Dinda, JCAP 09, 062, arXiv:2405.06618 [astro-ph.CO].
- [173] M. Najafi, S. Pan, E. Di Valentino, and J. T. Firouzjaee, Phys. Dark Univ. 45, 101539 (2024), arXiv:2407.14939 [astro-ph.CO].
- [174] H. Wang and Y.-S. Piao, Dark energy in light of recent DESI BAO and Hubble tension (2024), arXiv:2404.18579 [astro-ph.CO].
- [175] G. Ye, M. Martinelli, B. Hu, and A. Silvestri, Phys. Rev. Lett. 134, 181002 (2025), arXiv:2407.15832 [astro-ph.CO].
- [176] Y. Tada and T. Terada, Phys. Rev. D 109, L121305 (2024), arXiv:2404.05722 [astro-ph.CO].
- [177] Y. Carloni, O. Luongo, and M. Muccino, Phys. Rev. D

- 111, 023512 (2025), arXiv:2404.12068 [astro-ph.CO].
- [178] C.-G. Park, J. de Cruz Pérez, and B. Ratra, Phys. Rev. D 110, 123533 (2024), arXiv:2405.00502 [astro-ph.CO].
- [179] K. Lodha et al. (DESI), Phys. Rev. D 111, 023532 (2025), arXiv:2405.13588 [astro-ph.CO].
- [180] S. Bhattacharya, G. Borghetto, A. Malhotra, S. Parameswaran, G. Tasinato, and I. Zavala, JCAP 09, 073, arXiv:2405.17396 [astro-ph.CO].
- [181] O. F. Ramadan, J. Sakstein, and D. Rubin, Phys. Rev. D 110, L041303 (2024), arXiv:2405.18747 [astro-ph.CO].
- [182] A. Notari, M. Redi, and A. Tesi, JCAP 11, 025, arXiv:2406.08459 [astro-ph.CO].
- [183] L. Orchard and V. H. Cárdenas, Phys. Dark Univ. 46, 101678 (2024), arXiv:2407.05579 [astro-ph.CO].
- [184] A. Hernández-Almada, M. L. Mendoza-Martínez, M. A. García-Aspeitia, and V. Motta, Phys. Dark Univ. 46, 101668 (2024), arXiv:2407.09430 [astro-ph.CO].
- [185] S. Pourojaghi, M. Malekjani, and Z. Davari, Cosmological constraints on dark energy parametrizations after DESI 2024: Persistent deviation from standard ΛCDM cosmology (2024), arXiv:2407.09767 [astro-ph.CO].
- [186] W. Giarè, M. Najafi, S. Pan, E. Di Valentino, and J. T. Firouzjaee, JCAP 10, 035, arXiv:2407.16689 [astro-ph.CO].
- [187] J. a. Rebouças, D. H. F. de Souza, K. Zhong, V. Miranda, and R. Rosenfeld, JCAP 02, 024, arXiv:2408.14628 [astro-ph.CO].
- [188] W. Giarè, Dynamical Dark Energy Beyond Planck? Constraints from multiple CMB probes, DESI BAO and Type-Ia Supernovae (2024), arXiv:2409.17074 [astro-ph.CO].
- [189] C.-G. Park, J. de Cruz Perez, and B. Ratra, Is the w_0w_a CDM cosmological parameterization evidence for dark energy dynamics partially caused by the excess smoothing of Planck CMB anisotropy data? (2024), arXiv:2410.13627 [astro-ph.CO].
- [190] N. Menci, A. A. Sen, and M. Castellano, Astrophys. J. 976, 227 (2024), arXiv:2410.22940 [astro-ph.CO].
- [191] T.-N. Li, Y.-H. Li, G.-H. Du, P.-J. Wu, L. Feng, J.-F. Zhang, and X. Zhang, Revisiting holographic dark energy after DESI 2024 (2024), arXiv:2411.08639 [astro-ph.CO].
- [192] J.-X. Li and S. Wang, A comprehensive numerical study on four categories of holographic dark energy models (2024), arXiv:2412.09064 [astro-ph.CO].
- [193] A. Notari, M. Redi, and A. Tesi, BAO vs. SN evidence for evolving dark energy (2024), arXiv:2411.11685 [astro-ph.CO].
- [194] Q. Gao, Z. Peng, S. Gao, and Y. Gong, Universe 11, 10 (2025), arXiv:2411.16046 [astro-ph.CO].
- [195] R. Fikri, E. ElKhateeb, E. S. Lashin, and W. El Hanafy, A preference for dynamical phantom dark energy using one-parameter model with Planck, DESI DR1 BAO and SN data (2024), arXiv:2411.19362 [astro-ph.CO].
- [196] J. Zheng, D.-C. Qiang, and Z.-Q. You, Cosmological constraints on dark energy models using DESI BAO 2024 (2024), arXiv:2412.04830 [astro-ph.CO].
- [197] S. Roy Choudhury and T. Okumura, Astrophys. J. Lett. 976, L11 (2024), arXiv:2409.13022 [astro-ph.CO].
- [198] C. Li, J. Wang, D. Zhang, E. N. Saridakis, and Y.-F. Cai, JCAP 08, 041, arXiv:2504.07791 [astro-ph.CO].
- [199] A. Lewis and E. Chamberlain, Understanding acoustic scale observations: the one-sided fight against Λ (2024),

- arXiv:2412.13894 [astro-ph.CO].
- [200] W. J. Wolf, C. García-García, and P. G. Ferreira, Robustness of Dark Energy Phenomenology Across Different Parameterizations (2025), arXiv:2502.04929 [astroph.CO].
- [201] A. J. Shajib and J. A. Frieman, Evolving dark energy models: Current and forecast constraints (2025), arXiv:2502.06929 [astro-ph.CO].
- [202] W. Giarè, T. Mahassen, E. Di Valentino, and S. Pan, Phys. Dark Univ. 48, 101906 (2025), arXiv:2502.10264 [astro-ph.CO].
- [203] E. Chaussidon et al., Early time solution as an alternative to the late time evolving dark energy with DESI DR2 BAO (2025), arXiv:2503.24343 [astro-ph.CO].
- [204] D. A. Kessler, L. A. Escamilla, S. Pan, and E. Di Valentino, One-parameter dynamical dark energy: Hints for oscillations (2025), arXiv:2504.00776 [astro-ph.CO].
- [205] Y.-H. Pang, X. Zhang, and Q.-G. Huang, The Impact of the Hubble Tension on the Evidence for Dynamical Dark Energy (2025), arXiv:2503.21600 [astro-ph.CO].
- [206] N. Roy, Phys. Dark Univ. 48, 101912 (2025), arXiv:2406.00634 [astro-ph.CO].
- [207] S. Roy Choudhury, Cosmology in Extended Parameter Space with DESI DR2 BAO: A $2\sigma+$ Detection of Non-zero Neutrino Masses with an Update on Dynamical Dark Energy and Lensing Anomaly (2025), arXiv:2504.15340 [astro-ph.CO].
- [208] A. Paliathanasis, Phys. Dark Univ. 48, 101956 (2025), arXiv:2502.16221 [astro-ph.CO].
- [209] W. Giarè, Phys. Rev. D 112, 023508 (2025), arXiv:2409.17074 [astro-ph.CO].
- [210] T. Liu, X. Li, and J. Wang, Astrophys. J. 988, 243 (2025), arXiv:2504.21373 [astro-ph.CO].
- [211] E. M. Teixeira, W. Giarè, N. B. Hogg, T. Montandon, A. Poudou, and V. Poulin, Implications of distance duality violation for the H₀ tension and evolving dark energy (2025), arXiv:2504.10464 [astro-ph.CO].
- [212] F. B. M. d. Santos, J. Morais, S. Pan, W. Yang, and E. Di Valentino, A New Window on Dynamical Dark Energy: Combining DESI-DR2 BAO with future Gravitational Wave Observations (2025), arXiv:2504.04646 [astro-ph.CO].
- [213] M. A. Sabogal and R. C. Nunes, Robust Evidence for Dynamical Dark Energy from DESI Galaxy-CMB Lensing Cross-Correlation and Geometric Probes (2025), arXiv:2505.24465 [astro-ph.CO].
- [214] H. Cheng, E. Di Valentino, L. A. Escamilla, A. A. Sen, and L. Visinelli, Pressure Parametrization of Dark Energy: First and Second-Order Constraints with Latest Cosmological Data (2025), arXiv:2505.02932 [astroph.CO].
- [215] L. Herold and T. Karwal, Bayesian and frequentist perspectives agree on dynamical dark energy (2025), arXiv:2506.12004 [astro-ph.CO].
- [216] H. Cheng, E. Di Valentino, and L. Visinelli, Cosmic Strings as Dynamical Dark Energy: Novel Constraints (2025), arXiv:2505.22066 [astro-ph.CO].
- [217] A. N. Ormondroyd, W. J. Handley, M. P. Hobson, and A. N. Lasenby, Comparison of dynamical dark energy with ΛCDM in light of DESI DR2 (2025), arXiv:2503.17342 [astro-ph.CO].
- [218] E. Silva and R. C. Nunes, Testing Signatures of Phantom Crossing through Full-Shape Galaxy Clustering

- Analysis (2025), arXiv:2507.13989 [astro-ph.CO].
- [219] M. Ishak and L. Medina-Varela, Is this the fall of the LCDM throne? Evidence for dynamical dark energy rising from combinations of different types of datasets (2025), arXiv:2507.22856 [astro-ph.CO].
- [220] E. Fazzari, W. Giarè, and E. Di Valentino, Cosmographic Footprints of Dynamical Dark Energy (2025), arXiv:2509.16196 [astro-ph.CO].
- [221] N. Arendse et al., Astron. Astrophys. 639, A57 (2020), arXiv:1909.07986 [astro-ph.CO].
- [222] L. Hart and J. Chluba, Mon. Not. Roy. Astron. Soc. 519, 3664 (2023), arXiv:2209.12290 [astro-ph.CO].
- [223] J. Chluba and L. Hart, Varying fundamental constants meet Hubble (2023), arXiv:2309.12083 [astro-ph.CO].
- [224] Y. Toda and O. Seto, Phys. Dark Univ. 49, 102035 (2025), arXiv:2504.09136 [astro-ph.CO].
- [225] Y. Toda and O. Seto, Constraints on the varying electron mass and early dark energy in light of ACT DR6 and DESI DR2 and the implications for inflation (2025), arXiv:2508.09025 [astro-ph.CO].
- [226] Y.-Y. Wang, L. Lei, S.-P. Tang, and Y.-Z. Fan, Lensing amplitude anomaly and varying electron mass alleviate the Hubble and S_8 tensions (2025), arXiv:2508.19081 [astro-ph.CO].
- [227] M. Chevallier and D. Polarski, Int. J. Mod. Phys. D 10, 213 (2001), arXiv:gr-qc/0009008.
- [228] E. V. Linder, Phys. Rev. Lett. 90, 091301 (2003), arXiv:astro-ph/0208512.
- [229] Y.-F. Cai, E. N. Saridakis, M. R. Setare, and J.-Q. Xia, Phys. Rept. 493, 1 (2010), arXiv:0909.2776 [hep-th].
- [230] R. R. Caldwell and E. V. Linder, Phys. Rev. Lett. 95, 141301 (2005), arXiv:astro-ph/0505494.
- [231] R. J. Scherrer and A. Sen, Phys. Rev. D 77, 083515 (2008), arXiv:0712.3450 [astro-ph].
- [232] W. J. Wolf, C. García-García, D. J. Bartlett, and P. G. Ferreira, Phys. Rev. D 110, 083528 (2024), arXiv:2408.17318 [astro-ph.CO].
- [233] W. J. Wolf, P. G. Ferreira, and C. García-García, Phys. Rev. D 111, L041303 (2025), arXiv:2409.17019 [astro-ph.CO].
- [234] W. J. Wolf, C. García-García, T. Anton, and P. G. Ferreira, Phys. Rev. Lett. 135, 081001 (2025), arXiv:2504.07679 [astro-ph.CO].
- [235] K. Lodha et al. (DESI), Extended Dark Energy analysis using DESI DR2 BAO measurements (2025), arXiv:2503.14743 [astro-ph.CO].
- [236] R. E. Keeley, A. Shafieloo, and W. L. Matthewson, Could We Be Fooled about Phantom Crossing? (2025), arXiv:2506.15091 [astro-ph.CO].
- [237] N. Roy and S. Chakrabarti, Is Phantom Barrier Crossing Inevitable? A Cosmographic Analysis (2025), arXiv:2508.13740 [astro-ph.CO].
- [238] R. Chen, J. M. Cline, V. Muralidharan, and B. Salewicz, Quintessential dark energy crossing the phantom divide (2025), arXiv:2508.19101 [astro-ph.CO].
- [239] S. L. Guedezounme, B. R. Dinda, and R. Maartens, Phantom crossing or dark interaction? (2025), arXiv:2507.18274 [astro-ph.CO].
- [240] I. J. Allali, M. P. Hertzberg, and F. Rompineve, Phys. Rev. D 104, L081303 (2021), arXiv:2104.12798 [astro-ph.CO].
- [241] L. A. Anchordoqui, E. Di Valentino, S. Pan, and W. Yang, JHEAp 32, 28 (2021), arXiv:2107.13932 [astro-ph.CO].

- [242] N. Khosravi and M. Farhang, Phys. Rev. D 105, 063505 (2022), arXiv:2109.10725 [astro-ph.CO].
- [243] S. J. Clark, K. Vattis, J. Fan, and S. M. Koushiappas, Phys. Rev. D 107, 083527 (2023), arXiv:2110.09562 [astro-ph.CO].
- [244] H. Wang and Y.-S. Piao, Phys. Lett. B 832, 137244 (2022), arXiv:2201.07079 [astro-ph.CO].
- [245] L. A. Anchordoqui, V. Barger, D. Marfatia, and J. F. Soriano, Phys. Rev. D 105, 103512 (2022), arXiv:2203.04818 [astro-ph.CO].
- [246] A. Reeves, L. Herold, S. Vagnozzi, B. D. Sherwin, and E. G. M. Ferreira, Mon. Not. Roy. Astron. Soc. 520, 3688 (2023), arXiv:2207.01501 [astro-ph.CO].
- [247] Y.-H. Yao and X.-H. Meng, Commun. Theor. Phys. 76, 075401 (2024), arXiv:2312.04007 [astro-ph.CO].
- [248] S. S. da Costa, D. R. da Silva, A. S. de Jesus, N. Pinto-Neto, and F. S. Queiroz, JCAP 04, 035, arXiv:2311.07420 [astro-ph.CO].
- [249] M. S. Madhavacheril et al. (ACT), Astrophys. J. 962, 113 (2024), arXiv:2304.05203 [astro-ph.CO].
- [250] L. Balkenhol et al. (SPT-3G), Phys. Rev. D 109, 083506 (2024), arXiv:2308.11608.
- [251] D. Collaboration, In preparation (2025), arXiv:2506.XXXXX.
- [252] S. Alam et al. (BOSS), Mon. Not. Roy. Astron. Soc. 470, 2617 (2017), arXiv:1607.03155.
- [253] D. Brout et al., Astrophys. J. 938, 110 (2022), arXiv:2202.04077 [astro-ph.CO].
- [254] J.-P. Uzan, Living Rev. Rel. 14, 2 (2011), arXiv:1009.5514 [astro-ph.CO].
- [255] T. Damour and A. M. Polyakov, Nucl. Phys. B 423, 532 (1994), arXiv:hep-th/9401069.
- [256] M. Gasperini and G. Veneziano, Phys. Rept. 373, 1 (2003), arXiv:hep-th/0207130.
- [257] T. R. Taylor and G. Veneziano, Phys. Lett. B 213, 450 (1988).
- [258] A. Smith, M. Mylova, P. Brax, C. van de Bruck, C. Burgess, and A.-C. Davis, Journal of Cosmology and Astroparticle Physics 2025 (07), 023.
- [259] P. Brax, C. P. Burgess, and F. Quevedo, JCAP 08, 011, arXiv:2212.14870 [hep-ph].
- [260] C. P. Burgess, D. Dineen, and F. Quevedo, JCAP 03 (03), 064, arXiv:2111.07286 [hep-th].
- [261] M. Pietroni, Phys. Rev. D 72, 043535 (2005), arXiv:astro-ph/0505615.
- [262] K. A. Olive and M. Pospelov, Phys. Rev. D 65, 085044 (2002), arXiv:hep-ph/0110377.
- [263] C. Wetterich, Nucl. Phys. B 302, 668 (1988), arXiv:1711.03844 [hep-th].
- [264] B. Patt and F. Wilczek (2006), arXiv:hep-ph/0605188.
- [265] R. M. Schabinger and J. D. Wells, Phys. Rev. D 72, 093007 (2005), arXiv:hep-ph/0509209.
- [266] C. Englert, T. Plehn, D. Zerwas, and P. M. Zerwas, Phys. Lett. B 703, 298 (2011), arXiv:1106.3097 [hep-ph].
- [267] C. Burrage and P. Millington, Annals N. Y. Acad. Sci. 1531, 95 (2024), arXiv:2310.12071 [hep-ph].
- [268] J. Khoury and A. Weltman, Phys. Rev. Lett. 93, 171104 (2004), arXiv:astro-ph/0309300.
- [269] P. Brax, C. van de Bruck, A.-C. Davis, J. Khoury, and A. Weltman, Phys. Rev. D 70, 123518 (2004), arXiv:astro-ph/0408415.
- [270] H. B. Sandvik, J. D. Barrow, and J. Magueijo, Phys. Rev. Lett. 88, 031302 (2002), arXiv:astro-ph/0107512.

- [271] J. D. Barrow, Phys. Rev. D 71, 083520 (2005), arXiv:astro-ph/0503434.
- [272] R. H. Cyburt, B. D. Fields, K. A. Olive, and T.-H. Yeh, Rev. Mod. Phys. 88, 015004 (2016), arXiv:1505.01076 [astro-ph.CO].
- [273] J. Chluba, G. Vasil, and R. Battye, Ito calculus meets the Hubble tension: Effects of small-scale electron density fluctuations on the CMB anisotropies (2025), arXiv:2505.22242 [astro-ph.CO].
- [274] W. J. Wolf and P. G. Ferreira, Phys. Rev. D 108, 103519 (2023), arXiv:2310.07482 [astro-ph.CO].
- [275] C. R. Watson and R. J. Scherrer, Phys. Rev. D 68, 123524 (2003), arXiv:astro-ph/0306364.
- [276] T. Chiba, Phys. Rev. D 81, 023515 (2010), arXiv:0909.4365 [astro-ph.CO].
- [277] S. Dutta and R. J. Scherrer, Phys. Lett. B 704, 265 (2011), arXiv:1106.0012 [astro-ph.CO].
- [278] C. Wetterich, Astron. Astrophys. **301**, 321 (1995), arXiv:hep-th/9408025.
- [279] L. Amendola, Phys. Rev. D 62, 043511 (2000), arXiv:astro-ph/9908023.
- [280] J. Khoury and A. Weltman, Phys. Rev. D 69, 044026 (2004), arXiv:astro-ph/0309411.
- [281] S. Das, P. S. Corasaniti, and J. Khoury, Phys. Rev. D 73, 083509 (2006), arXiv:astro-ph/0510628.
- [282] C. van de Bruck and J. Morrice, JCAP **04**, 036, arXiv:1501.03073 [gr-qc].
- [283] G.-B. Zhao et al., Nature Astron. 1, 627 (2017), arXiv:1701.08165 [astro-ph.CO].
- [284] E. Di Valentino, A. Melchiorri, and J. Silk, Phys. Lett. B 761, 242 (2016), arXiv:1704.00762 [astro-ph.CO].
- [285] G. Alestas, L. Kazantzidis, and L. Perivolaropoulos, Phys. Rev. D 101, 123516 (2020), arXiv:2004.08363 [astro-ph.CO].
- [286] S. Nesseris, Y. Akrami, and G. D. Starkman, To CPL, or not to CPL? What we have not learned about the dark energy equation of state (2025), arXiv:2503.22529 [astro-ph.CO].
- [287] A. Gómez-Valent and A. González-Fuentes, Effective Phantom Divide Crossing with Standard and Negative Quintessence (2025), arXiv:2508.00621 [astro-ph.CO].
- [288] R. Calderon *et al.* (DESI), JCAP **10**, 048, arXiv:2405.04216 [astro-ph.CO].
- [289] A. González-Fuentes and A. Gómez-Valent, Reconstruction of dark energy and late-time cosmic expansion using the Weighted Function Regression method (2025), arXiv:2506.11758 [astro-ph.CO].
- [290] N. Aghanim et al. (Planck), Astron. Astrophys. 641, A5 (2020), arXiv:1907.12875 [astro-ph.CO].
- [291] F. J. Qu et al. (ACT), Astrophys. J. 962, 112 (2024), arXiv:2304.05202 [astro-ph.CO].
- [292] J. Carron, M. Mirmelstein, and A. Lewis, JCAP 09, 039, arXiv:2206.07773 [astro-ph.CO].
- [293] F. J. Qu et al. (SPT-3G, ACT), Unified and consistent structure growth measurements from joint ACT, SPT and \textitPlanck CMB lensing (2025), arXiv:2504.20038 [astro-ph.CO].
- [294] M. Abdul Karim et al. (DESI), arXiv:2503.14739 [astro-ph.CO] (2025).
- [295] S. Alam et al. (eBOSS), Phys. Rev. D 103, 083533 (2021), arXiv:2007.08991 [astro-ph.CO].
- [296] D. Blas, J. Lesgourgues, and T. Tram, Journal of Cosmology and Astroparticle Physics 2011 (07), 034–034.
- [297] J. Torrado and A. Lewis, JCAP 05, 057,

- arXiv:2005.05290 [astro-ph.IM].
- [298] Y. Ali-Haïmoud and C. M. Hirata, Physical Review D 83, 10.1103/physrevd.83.043513 (2011).
- [299] W. Hu and I. Sawicki, Phys. Rev. D 76, 104043 (2007), arXiv:0708.1190 [astro-ph].
- [300] A. Lewis, GetDist: a Python package for analysing Monte Carlo samples (2019), arXiv:1910.13970 [astroph.IM].
- [301] M. Raveri and W. Hu, Phys. Rev. D 99, 043506 (2019), arXiv:1806.04649 [astro-ph.CO].
- [302] M. Raveri and C. Doux, Phys. Rev. D 104, 043504 (2021), arXiv:2105.03324 [astro-ph.CO].
- [303] M. Artola, I. Ayuso, R. Lazkoz, and V. Salzano, arXiv:2510.04191 [astro-ph.CO] (2025).
- [304] B. Hu, M. Raveri, N. Frusciante, and A. Silvestri, Phys. Rev. D 89, 103530 (2014), arXiv:1312.5742 [astroph.CO].
- [305] W. Fang, W. Hu, and A. Lewis, Phys. Rev. D 78, 087303 (2008), arXiv:0808.3125 [astro-ph].
- [306] W. Hu, Phys. Rev. D 71, 047301 (2005), arXiv:astro-ph/0410680.
- [307] T. Kobayashi, Rept. Prog. Phys. 82, 086901 (2019), arXiv:1901.07183 [gr-qc].
- [308] S. Tsujikawa, arXiv:2508.17231 [astro-ph.CO] (2025).
- [309] H. Wei, R.-G. Cai, and D.-F. Zeng, Class. Quant. Grav. 22, 3189 (2005), arXiv:hep-th/0501160.
- [310] P. Brax, arXiv:2507.16723 [astro-ph.CO] (2025).
- [311] A. Smith, P. Brax, C. van de Bruck, C. P. Burgess, and A.-C. Davis, Eur. Phys. J. C 85, 1062 (2025), arXiv:2505.05450 [hep-th].
- [312] D. Langlois, Int. J. Mod. Phys. D 28, 1942006 (2019), arXiv:1811.06271 [gr-qc].
- [313] Y. Tiwari, U. Upadhyay, and R. K. Jain, Phys. Rev. D 111, 043530 (2025), arXiv:2412.00931 [astro-ph.CO].

Appendix A: Comparison of Priors

Our constraints on various parameters, in particular the inferred value of H_0 for the CPL+ m_e model, differ from those obtained in [163]. In this appendix, we investigate the cause of this discrepancy. For direct comparability with [163], we remove the ACT DR6 lensing data from our CMB combination and focus on the impact of the prior choice on w_a .

Table V shows the 68% confidence intervals on the $CPL+m_e$ model when imposing a wide flat prior (-3 < $w_a < 2$) compared to the narrower prior $(-1 < w_a < 1)$ adopted in [163]. Allowing a wider region in the w_a parameter space shifts the posterior support to more negative values. The right-hand panel of Fig. 7 illustrates why: when constraining with CMB-A+DESI+PP datasets, w_a remains unconstrained toward increasingly negative values, and imposing $w_a > -1$ artificially truncates this flat direction. This truncation affects not only w_a , but also propagates through its degeneracies with H_0 and $m_e/m_{e,0}$. More negative w_a values correlate with higher Ω_m and lower H_0 and $m_e/m_{e,0}$, as can be seen in the elongated degeneracy directions in Fig. 7. Cutting the tail of this degeneracy at $w_a = -1$ removes the region with low H_0 corresponding to low $m_e/m_{e,0}$ and high Ω_m ,

Parameter		$CPL + m_e (-1 < w_a < 1)$
$m_e/m_{e,0}$	$0.9976^{+0.0070}_{-0.0089}$	$1.0052^{+0.0081}_{-0.0093}$
$w_{0,\mathrm{DE}}$	$-0.45^{+0.34}_{-0.18}$	$-0.89^{+0.19}_{-0.12}$
$w_{a,\mathrm{DE}}$	< -1.56	< -0.359
$H_0({\rm km s^{-1} Mpc^{-1}})$		$69.0^{+1.9}_{-2.7}$
$\Omega_{ m m} h^2$	$0.1425^{+0.0020}_{-0.0023}$	0.1437 ± 0.0023
σ_8	$0.793^{+0.022}_{-0.030}$	$0.824^{+0.022}_{-0.025}$
$\frac{\sigma_8}{\chi^2}$	2790.7 ± 6.4	2794.4 ± 6.3

TABLE V. Comparison of parameter constraints at the 68% confidence level from the $CPL+m_e$ model using the CMB-A+DESI dataset combination (excluding ACT DR6 lensing, unlike the rest of the paper), under different prior choices for w_a .

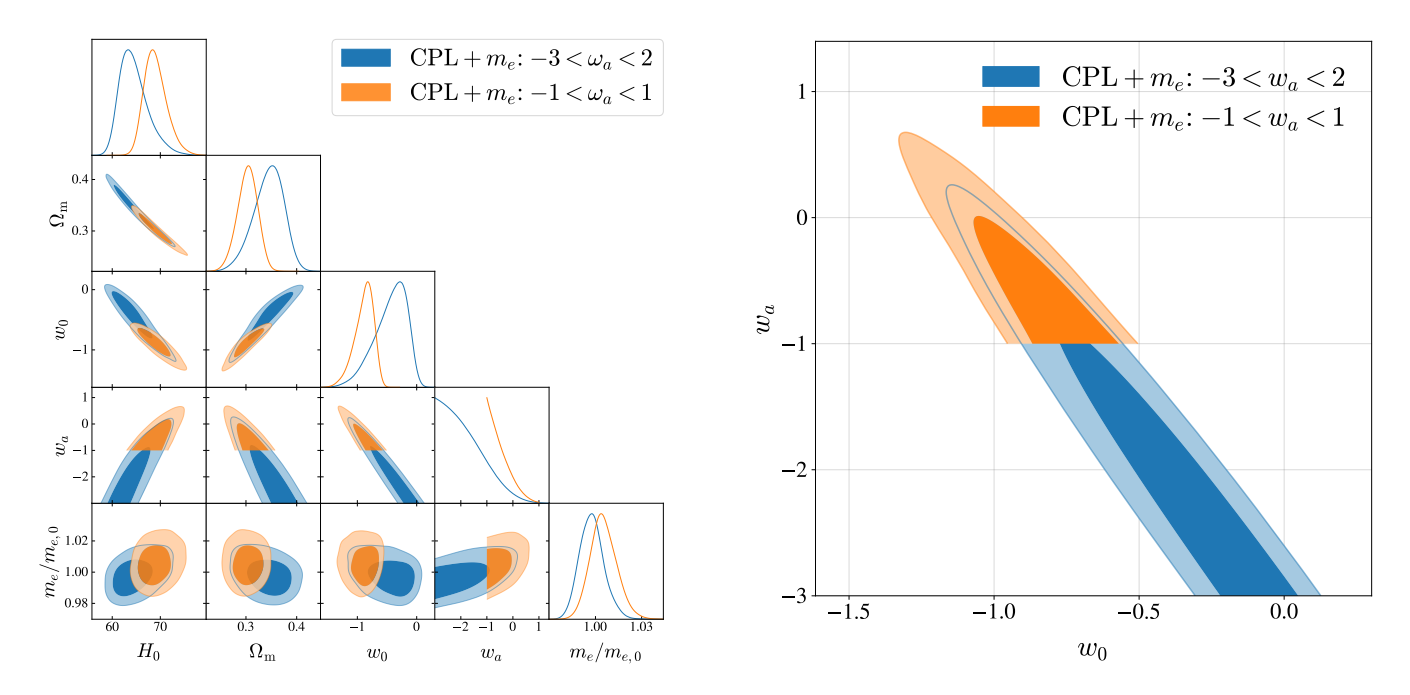


FIG. 7. Comparison of posterior distributions for the CPL + m_e model using the CMB-A+DESI dataset combination, but excluding ACT DR6 lensing. Shown are the 68% and 95% confidence regions for key parameters under two prior choices: wide $(-3 < w_a < 2$, blue) and narrow $(-1 < w_a < 1$, orange). The narrower prior truncates the degeneracy direction toward more negative w_a , thereby removing regions with lower H_0 and higher Ω_m , and shifting the preferred parameter values.

shifting the marginalised posteriors. It remains to be seen if the priors used in this work are broad enough. Such a bias could also impact one's conclusions on fundamental physics; as can be seen from comparing the contours in Fig. 7, the narrower prior also leads to a better agreement with the ΛCDM -like late time evolution.

In practice, this explains why analyses that adopt $-1 < w_a < 1$ (as in [163]) find $H_0 \simeq 69 \text{ km s}^{-1} \text{ Mpc}^{-1}$, whereas with a broader prior the same datasets allow values closer to $H_0 \simeq 65 \text{ km s}^{-1} \text{ Mpc}^{-1}$. Broadening the prior reveals a larger extent of the parameter space, while

restricting the prior artificially suppresses the correlated region and biases the apparent constraints on H_0 .

This exercise demonstrates that prior choices on w_a are not innocuous in CPL-like models once strong degeneracies are present. Analyses adopting $-1 < w_a < 1$ (as in [163]) will inevitably push posteriors toward higher H_0 relative to those obtained with broader priors, explaining the apparent discrepancy between our findings and theirs. Moreover, even for our priors, the posterior accumulates at the border of the prior in this example, implying these results may also be suffering from a similar bias, and broadening the prior range further may shift the results.